Biogeosciences Discuss., https://doi.org/10.5194/bg-2018-261
Manuscript under review for journal Biogeosciences
Discussion started: 21 June 2018

Biogeosciences Discussions Open Access EGU

Patterns of suspended particulate matter across the continental margin in the Canadian Beaufort Sea

Jens K. Ehn[1], Rick A. Reynolds[2], Dariusz Stramski[2], David Doxaran[3], and Marcel Babin[4]

[1]Centre for Earth Observation Science, University of Manitoba, Winnipeg, Manitoba, Canada.
[2]Marine Physical Laboratory, Scripps Institution of Oceanography, University of California San Diego, La Jolla, California, U.S.A.
[3]Sorbonne Université, CNRS, Laboratoire d'Océanographie de Villefanche, Villefranche-sur-mer 06230, France.
[4]Joint International ULaval-CNRS Laboratory Takuvik, Québec-Océan, Département de Biologie, Université Laval, Québec, Québec, Canada.

Correspondence: Jens K. Ehn (jens.ehn@umanitoba.ca)

Abstract. The particulate beam attenuation coefficient at 660 nm, $c_{\mathrm{p}}(660)$, was measured in conjunction with properties of suspended particle assemblages in August 2009 within the Canadian Beaufort Sea continental margin, a region heavily influenced by sediment discharge from the Mackenzie River. The suspended particulate matter mass concentration (SPM) ranged from 0.04 to 140 g m^{-3}, its composition varied from mineral to organic-dominated, and the median particle diameter ranged determined over the range 0.7–120 μm varied from 0.78 to 9.45 μm, with the fraction of particles < 1 μm highest in surface layers influenced by river water or ice melt. A relationship between SPM and $c_{\mathrm{p}}(660)$ was developed and used to determine SPM distributions based on measurements of $c_{\mathrm{p}}(660)$ taken during summer seasons of 2004, 2008 and 2009, as well as fall 2007. SPM spatial patterns on the shelf are explained by an interplay between wind forcing, river discharge, and sea ice coverage resulting in three circulation modes: shelfbreak upwelling, relaxation of upwelling, and vertical mixing. Offshore ice melt affected the river plume extent while meltwater on the shelf was associated with enhanced near-bottom SPM during upwelling return flow. SPM decreased sharply past the shelfbreak with further transport of particulate matter occurring near the bottom and in interleaving nepheloid layers. The deepest nepheloid layer was observed near 2600 m depth, immediately below the transition to the Canada Basin Bottom Water mass. These findings expand our knowledge of particle distributions in the Beaufort Sea controlled by river discharge, sea ice, and wind, each of which is sensitive to weather and climate variations.

1 Introduction

The Canadian Beaufort Sea is subject to great seasonal and interannual variability in its sea ice coverage (Galley et al., 2008; Yang, 2009; Stroeve et al., 2014), freshwater input (McClelland et al., 2012), and atmospheric forcing (Yang, 2009; Asplin et al., 2012; Moore, 2012; Kirillov et al., 2016), all of which strongly influence the water circulation. In particular, the region includes the Canadian Beaufort Shelf, which is the most turbid of all shelf seas in the Arctic Ocean. High attenuation of solar radiation by both the ice and turbid seawater greatly limit primary productivity on the shelf (Carmack and Macdonald, 2002). The Canadian Beaufort Shelf is about 120 km wide, 500 km long, < 80 m deep, and is estimated to receive on average about

Biogeosciences Discuss., https://doi.org/10.5194/bg-2018-261
Manuscript under review for journal Biogeosciences
Discussion started: 21 June 2018

330 km^3 per year of freshwater from the Mackenzie River with a sediment load of 130 Mt per year (Macdonald et al., 1998; O'Brien et al., 2006). The significance of sediment discharge to the region is underscored by the fact that this sediment load surpasses the combined load of all other major rivers discharging into the Arctic Ocean. Additional sediment sources to the shelf include coastal and bottom erosion, and other rivers, which have been estimated to provide ∼9 Mt per year (Macdonald et al., 1998). The bulk of the sediment carried by the Mackenzie River is deposited in the delta (∼50 % of input) and on the shelf (∼40 %); however, a poorly known fraction of particles is transported across the shelfbreak carried either in surface river plumes, near the bottom in nepheloid layers, or by ice rafting (Macdonald et al., 1998). Resuspension of sediments settled on the shelf bottom are thought to play a significant role in the cross-shelf transport in the nepheloid layers (O'Brien et al., 2011).

Additionally, marine phytoplankton production, including the contribution by sea-ice associated algae towards the end of the ice-covered season, is a major source of biogenous particles in the Beaufort Sea during summer (Forest et al., 2007, 2010; Tremblay et al., 2008). The particulate sinking flux therefore comprises highly variable fractions of allochthonous and autochthonous origins (Sallon et al., 2011), making particle characterization in the area a complex task. The vertical export of autochtonous organic material to the deep waters of Canada Basin is found to be surprisingly small, however (Honjo et al., 2010). As the organic material reaching the deep ocean layers is thousands of years old it must be transported there laterally from the shelf or slope reservoirs of highly refractory material (Honjo et al., 2010). This highlights the importance of understanding the distribution and lateral transport of particulate material from the shelf.

The mechanisms and pathways of cross-shelf and slope particle transport in the Canadian Beaufort Sea remain poorly understood (O'Brien et al., 2011). This is largely because of a lack of data of sufficient resolution; biogeochemically important constituents in such a large and dynamic system are difficult to characterize with traditional methods that rely on discrete water sampling. To infer particle transport pathways, a description of the distribution and variability of particle concentrations associated with the factors controlling the water circulation is required. Ocean color remote sensing of suspended particles provides a much better spatial coverage, but is limited to surface waters. In situ optical techniques, most commonly involving a measurement of beam attenuation coefficient, allow a significant increase in observational time and space scales. Because beam attenuation is sensitive not only to the concentration of particles but also their size and composition, numerous relationships have been developed to relate the particulate beam attenuation coefficient, $c_\mathrm{p}(\lambda)$ (where λ is light wavelength in vacuo) to the dry mass concentration of suspended particulate matter (SPM) and particulate organic carbon (POC) (e.g., Bishop, 1986, 1999; Bunt et al., 1999; Gardner et al., 2006; Stramski et al., 2008; Jackson et al., 2010; Hill et al., 2011). The beam attenuation at light wavelength of 660 nm has been typically used in these relationships.

Because of various origins and variable composition of particle assemblages in the southeastern Beaufort Sea, the feasibility of inferring SPM and POC from beam attenuation has been questioned for this region (Jackson et al., 2010). Nevertheless, in this study we use a comprehensive set of field data collected as part of MALINA project in summer 2009 in waters with diverse composition of particulate matter characterized by variation in the ratio of POC/SPM to determine statistical relationships between the particulate beam attenuation coefficient at 660 nm, $c_\mathrm{p}(660)$, and SPM and POC. These relationships are then applied to infer the particle concentration fields from measurements of beam attenuation taken during cruises to the Canadian Beaufort Sea associated with the MALINA project as well as four other projects. Although we recognize the possibility of interannual

and seasonal variability in particle characteristics, our analysis aims at deriving information on how particle distributions along transects crossing the Canadian Beaufort Sea continental margin into the Canada Basin during the open water season are linked to oceanographic conditions, and affected by wind forcing, river discharge and sea ice coverage.

2 Materials and Methods

2.1 MALINA sampling overview

The MALINA expedition was conducted from 31 July to 24 August 2009 in the southeastern Beaufort Sea on the research icebreaker *CCGS Amundsen*. A total of 167 CTD/Rosette casts were carried out during the expedition with water sampling conducted at 28 station locations (Fig. 1). A small barge was launched to conduct coincident surface water sampling away from the ship's influence on 26 of these stations. In addition, the barge visited 12 additional stations in waters too shallow for the ship (Fig. 1; Doxaran et al., 2012). The CTD/Rosette onboard the icebreaker was equipped with 24 12-liter Niskin bottles for water collection and various in situ instruments including an SBE-911plus CTD (Sea-bird Electronics, Inc.), a C-Star 25-cm beam transmissometer (Wetlabs, Inc.) for measuring particulate beam attenuation coefficient at 660 nm, $c_{\mathrm{p}}(660)$ in units of m^{-1}, and a Wetstar fluorometer (Wetlabs, Inc.) for measuring fluorescence of chlorophyll-*a* (chl-*a*).

In this study, the discussion is centered on the analysis and cross section plots for transect lines 100, 200, 300 and 600 only. Line 100 crossed the Amundsen Gulf near its entrance from north of Cape Bathurst towards the southwestern point of Banks Island. Lines 200 and 300 were south-to-north transects located approximately along 130° W and 134° W, respectively, with the latter associated with the Kugmallit Valley. The line 600 followed the Mackenzie Trough and provided the western border to the Mackenzie shelf. The Mackenzie River delta is a maze of channels; however, the main discharge channel exits at Mackenzie Bay near the end of line 600, while the second largest channel exits at Kugmallit Bay near line 300. Transect lines 100, 300, and 600 have been also repeatedly measured during other field campaigns (e.g., Carmack et al., 1989; Tremblay et al., 2011).

2.2 Determinations of SPM and POC

Water samples for SPM and POC determinations were collected at 28 CTD/Rosette stations and 38 barge stations (12 stations along two transects towards the Mackenzie River mouths and the remaining located in the vicinity of the ship stations (Fig. 1); see also Doxaran et al. (2012)). Niskin bottles were triggered during CTD/Rosette upcasts to collect water samples at 3 to 4 depths, which always included the near-surface water (1.5–3 m depth range) and subsurface chlorophyll-*a* maximum (SCM) if present. To ensure representative sampling of entire particle assemblages within Niskin bottles (including particles settled below the level of the spigot), the full content of the 12-liter Niskin bottles was drained directly into 20-liter HDPE carboys (Nalgene) by opening the bottom lid (Knap et al., 1996). Aliquots were then sampled from the carboys after mixing. If sufficient volume of water was available, filtration for SPM and POC determinations was made in triplicate for each examined depth. However, this was not always possible in clear waters with low particle concentrations, in which case either duplicates or single

Biogeosciences Discuss., https://doi.org/10.5194/bg-2018-261
Manuscript under review for journal Biogeosciences
Discussion started: 21 June 2018

samples were prepared. Water samples for SPM and POC on the barge were collected by directly submerging a 20-liter HDPE carboy below the seawater surface (Doxaran et al., 2012). Doxaran et al. (2012) reports on coefficient of variations for SPM and POC for these surface samples measured in triplicate. Additional near-surface water samples were occasionally collected by lowering a bucket from the side of the ship.

Water samples for SPM and POC were filtered through 25 mm diameter Whatman GF/F filters under low vacuum (leq 5 psi). Prior to the cruise the filters for both SPM and POC determinations had been rinsed with Milli-Q water, combusted at 450 °C for 1.5 hours to remove organic material, and weighed using a Mettler-Toledo MT5 balance ($\pm$0.001 mg precision) to obtain the blank measurement of the filter mass. Filters were stored individually in Petri dishes until the time of sample filtration. The volume of filtered seawater was adjusted to optimize particle load on the filter. This volume ranged from 0.2 L for very turbid samples collected near the Mackenzie River mouth (station 697) to 5.8 L at station 780. Immediately following filtration, filters were rinsed with about 50 mL of Milli-Q water to remove salts, transferred back to the Petri slides, and dried for 6-12 h at 55 °C. The dried filters were stored at -80 °C until processing. After the cruise, filters were again dried at 55 °C in the laboratory for about 24 h before measuring their dry weight using the same Mettler-Toledo MT5 balance. The SPM (in units of g m^{-3}) was determined by subtracting the blank filter mass from the sample filter mass and dividing by the volume of water filtered. The relative humidity of the room was about or below 40 % during weighing of filters to minimize the effect of uptake of moisture by the filters during the measurements. The protocol used for SPM determinations is consistent with standard methodology (e.g., Babin et al., 2003a).

SPM and POC were determined on the same GF/F filters. After the weighing for SPM, POC content was determined with an Organic Elemental Analyzer (PerkinElmer 2400 Series II CHNS/O) with a standard high-temperature combustion method as described in Doxaran et al. (2012). Prior to insertion of samples into the analyzer, the filters were acidified with 200-350 μL HCl 2N to remove inorganic carbon and then dried at 60 °C. Filters were compacted into small ($\sim$5 mm diameter) rounded pellets within pre-combusted aluminum foil. Blank filters for POC determinations were treated and measured in the same way as sample filters. The combustion temperature was kept at 925 °C. The final POC values (in units of g m^{-3}) were calculated by dividing the mass of organic carbon measured (in units of μg) on the sample filter (corrected for blank filter) by the filtered volume. In these calculations, the correction for blank filters was made using the average mass concentration of organic carbon determined on 9 blank filters, which was determined to be 21.2 μg (corresponding to a range of $\sim$2 to 50 % of measured signal for the sample filters; standard deviation was 8.1 μg).

2.3 Particle size distributions

The particle size distribution (PSD) of 54 discrete seawater samples collected with the CTD/Rosette or from the barge were measured using a Beckman-Coulter Multisizer III analyzer following the method described by Reynolds et al. (2016). In 40 of these samples, data were collected using both the 30 μm and 200 µm aperture sizes and merged into a single PSD ranging from 0.7 μm to 120 μm. Seawater filtered through a 0.2 μm filter was used as the diluent and blank, and multiple replicate measurements were acquired for each sample. Each aperture was calibrated using microsphere standards following recommendations by the manufacturer. The average number of particles per unit volume within each size class, N(D) (in units

Biogeosciences Discuss., https://doi.org/10.5194/bg-2018-261
Manuscript under review for journal Biogeosciences
Discussion started: 21 June 2018

of m^{-3}), where D is the midpoint diameter of the volume-equivalent sphere in each size class, was obtained after subtracting the counts for the blank. The particle volume distribution, V(D) (dimensionless), was then calculated from N(D) by assuming spherical particles.

2.4 Beam attenuation measurements

C-Star transmissometer data were recorded at 24 Hz as raw voltages and merged with the depth recording from the CTD/Rosette. Downcasts were processed to 1-m vertical bins centered at integers by averaging the interquartile range within bins. This method effectively removed spikes and noise from the data, if present. Time series of transmissometer data were also collected at selected depths and processed using the interquartile range method for the periods when the rosette was stopped during upcasts for water sampling with Niskin bottles. These data were used for correlational analysis with SPM and POC data from discrete Niskin bottle water samples. The particulate beam attenuation coefficient at 660 nm, $c_{\mathrm{p}}(660)$ (in units of m^{-1}), was then calculated from the binned voltage signal, V_{signal}, as

$$c_{\mathrm{p}}(660) = -\ln\left(\frac{V_{\mathrm{signal}} - V_{\mathrm{dark}}}{V_{\mathrm{ref}} - V_{\mathrm{dark}}}\right)/x \tag{1}$$

where x is the pathlength of 0.25 m, V_{dark} is the dark voltage offset, and V_{ref} is the reference voltage associated with particle free pure seawater (cf. C-Star User's Guide, Wetlabs, Inc.). For MALINA, V_{dark} was found to be 0.0517 V when measured immediately after a deep cast when the temperature of the instrument was equilibrated to seawater temperature. V_{ref} was taken as the highest V_{signal} reading observed during the expedition, i.e., it was determined to be 4.7362 V (lower than the factory supplied value of 4.8340 V) observed with the same instrument during the Geotraces cruise that followed immediately the MALINA cruise (cast 0903_26 on 4 September at depths between 1900 and 2500 m where water temperature and salinity averaged -0.40 °C and 34.94 PSU, respectively). This V_{ref} was only marginally higher than maximum values observed during the MALINA expedition. The above method also assumes a negligible contribution by CDOM to c_{p} at 660 nm (Bricaud et al., 1981), which is a reasonable assumption based on data shown in Matsuoka et al. (2012).

In this study we also use the C-Star transmissometer data obtained during CASES (2004), ArcticNet (2007) and IPY-CFL (2008) expeditions on the *CCGS Amundsen* (Ingram et al., 2008; Barber et al., 2010). The data were processed in the same way as the MALINA 2009 downcast data. One exception was that the factory supplied V_{dark} values were used exclusively as they had not been determined onboard the vessels. The V_{dark} values were 0.0570 V, 0.0574 V, and 0.0586 V for the CASES, ArcticNet, and IPY-CFL expeditions, respectively. The highest V_{signal} readings were 4.6783 V, 4.6498 V, and 4.7902 V, respectively. Four deep CTD casts were additionally collected in the Canada Basin during the Joint Ocean Ice Study (JOIS) on 21-23 September 2009 and the data were obtained from the Beaufort Gyre Exploration Program website (http://www.whoi.edu/beaufortgyre). These transmissometer data were processed as described above with a V_{dark} value of 0.0633 V (factory calibration) and V_{ref} value of 4.9408 V (maximum recorded value at station CB-21 on 9 October 2009).

Biogeosciences Discuss., https://doi.org/10.5194/bg-2018-261
Manuscript under review for journal Biogeosciences
Discussion started: 21 June 2018

2.5 Additional environmental data

To describe ocean currents, temperature, and salinity near the shelfbreak, we used, in addition to CTD casts, data from a current meter (RCM11, Aanderaa Instruments) moored at station CA05 near the center of Line 100 (Fig. 1). The locations where the mooring CA05 was deployed and the depth of the current meter varied slightly between years. During season 2003–2004, it was deployed in 250 m deep water (71.42° N, 127.37° W) at a depth of 202 m. In 2007–2008 and 2008–2009, the bottom depth was about 200 m (71.31° N, 127.60° W) and the instrument depth 178 m. In addition to current speed and direction, the instrument recorded water temperature, conductivity, turbidity, and dissolved oxygen content, all at 0.5 hour intervals. The conductivity sensor did not function in 2007–2008. For the 2008–2009 season, there was additionally a CT sensor (RBR Ltd.) with an integrated turbidity sensor (Seapoint Sensors, Inc.) deployed at a depth of 57 m from the surface and recording data at 10-minute intervals.

Annual estimates of Mackenzie River discharge and ice concentrations on the Canadian Beaufort Sea shelf for years 2004, 2007, 2008, and 2009 were obtained from publicly available data provided by Environment Canada. Daily discharge rates (in units of m3 s^{-1}) for the Mackenzie River at the Arctic Red River location (10LC014) were obtained from Water Survey of Canada (Environment Canada) hydrometric data online archives. Ice coverage with a 1-week resolution for the Mackenzie Shelf area was calculated using the IceGraph 2.0 program (region: cwa01_02) provided online by the Canadian Ice Service (Environment Canada).

Estimates of wind speed over the shelf were obtained by averaging 10-m elevation wind data over grid points located over the shelfbreak in the southeastern Beaufort Sea obtained from National Centers for Environmental Prediction (NCEP) (Fig. 1). As pointed out by Williams et al. (2006), NCEP data are readily available and may be preferable over observations made at coastal stations because the latter may be affected by the presence of land. We use the NCEP wind data in a qualitative sense to identify conditions that may have induced upwelling or downwelling of seawater within the shelf area (e.g., Kirillov et al., 2016).

3 Results and Discussion

3.1 Overview of water characteristics in August 2009

3.1.1 Water mass distributions

During the MALINA cruise in August 2009, there was a distinct east-west gradient in the observed surface salinity on the shelf (Fig. 2). To the west, surface salinities below 24 PSU were caused by the presence of the river plume that flowed along the coast and over the Mackenzie Trough in response to easterly winds during June 2009. The river plume formed a near-surface layer of about 15–20 m thickness, which covered the full extent of line 600 and line 700. To the east, water with salinity above 29 PSU was observed to reach the surface in the area north of Cape Bathurst. Williams and Carmack (2008) described such upwelling from within the Amundsen Gulf as topographically induced in response to easterly winds. Salinity values in excess

Biogeosciences Discuss., https://doi.org/10.5194/bg-2018-261
Manuscript under review for journal Biogeosciences
Discussion started: 21 June 2018

of 32 PSU were measured near the shelf bottom at 30 m (Fig. 2c), which correspond to Pacific waters in Amundsen Gulf at a depth of about 80 m (Fig. 2e). Generally, for the Canadian Beaufort Sea, salinity controls the vertical stratification such that higher salinity is found at greater depth. The salinity range between 30.7 and 32.3 PSU corresponds to the Pacific Summer Water mass, which as the name suggests originates from waters flowing through Bering Strait during summer (**?**Matsuoka et al., 2012). Underneath, the Pacific Winter Water is characterized by salinity between 32.3 and 33.9 PSU and typically found from ∼180 to 220 m depth. This is followed by a transition to waters of Atlantic-origin with salinity > 34.7 and temperature above 0 °C typically found between ∼220 and 800 m. Cold and dense deep water are found at greater depths and down to the bottom.

3.1.2 Beam attenuation and fluorescence

Generally, near-surface layer $c_{\mathrm{p}}(660)$ decreased from > 1 m^{-1} in coastal waters to < 0.02 m^{-1} in offshore Canada Basin waters (Fig. 2), reflecting the riverine and coastal sources of particulate matter. To the west, the fresher surface layer influenced by the river plume featured relatively high $c_{\mathrm{p}}(660)$ ranging from 0.1 to 0.4 m^{-1} (Fig. 2b) and high colored dissolved organic matter (CDOM) fluorescence (Fig. 3; Matsuoka et al., 2012). The highest ship-based observation of surface-water $c_{\mathrm{p}}(660)$ of ∼2.6 m^{-1} was observed at station 394 in 13-m deep waters at the mouth of Kugmallit Bay; however, reached 8.8 m^{-1} at 10 m depth and presumably higher values near the seabed. The surface waters in the area of upwelling just north of Cape Bathurst appear also to have been a hotspot in terms of particle concentration; $c_{\mathrm{p}}(660)$ at the surface of station 170 reached values over 1.2 m^{-1} (Fig. 2b).

The high $c_{\mathrm{p}}(660)$ values near the shelf seafloor in August 2009 were accompanied by a strong chl-*a* fluorescence signal, both of which also extended from the shelf far into the Canada Basin as a subsurface chl-*a* maximum (SCM) layer (Figs. 3a, c, e). The SCM layer is a consistent feature in the southern Beaufort Sea (Martin et al., 2010). The SCM was centered at depths between the 31.5 and 32.3 PSU isohalines, which corresponds to the lower portion of the Pacific Summer Water. The underlying Pacific Winter Water is characterized by maxima in both nutrients and CDOM (Fig. 3; Matsuoka et al., 2012). The nutrient maximum is typically found at the center of the Pacific Winter Water near the 33.1 PSU isohaline (Martin et al., 2010).

3.1.3 Particulate matter composition and size distribution

Empirical relationships between the beam attenuation coefficient and SPM are dependent on the composition and size distribution of particle assemblages (Kitchen et al., 1982; Bunt et al., 1999; Babin et al., 2003b; Reynolds et al., 2010; Woźniak et al., 2010; Hill et al., 2011), and may thus show regional differences. The proportion of organic to inorganic material is important because mineral particles have typically higher refractive index compared to organic particles, and thus generally produce higher scattering (e.g., Babin et al., 2003b; Woźniak et al., 2010). Beam attenuation is also affected by variable absorption. In particular, at 660 nm the absorption by chlorophyll pigments may cause important distinctions between organic and inorganic material (Doxaran et al., 2012; Bélanger et al., 2013). Particle size is of importance because the scattering cross-section of individual particles typically increases as particle size increases (Morel and Bricaud, 1986; Stramski and Kiefer, 1991). However, particle concentration often decreases significantly with an increase in particle size so that relatively small

particles can have higher contribution to bulk scattering per unit mass concentration of particles than larger particles (Babin et al., 2003b; Reynolds et al., 2010; Hill et al., 2011). In this section, we provide a description of the bulk composition and size distribution of particle assemblages sampled during the MALINA cruise in August 2009. The absorption associated with organic and inorganic material is described elsewhere (Doxaran et al., 2012; Bélanger et al., 2013). However, the measured particulate absorption at 660 nm was found to be smaller by 1–4 orders of magnitude than $c_{\mathrm{p}}(660)$ (data not shown).

Following Woźniak et al. (2010), the data representing discrete seawater samples were partitioned into three composition-related groups based on the POC/SPM ratio: 1) mineral-dominated when POC/SPM < 0.06, 2) mixed when 0.06 leq POC/SPM leq 0.25, and 3) organic-dominated when POC/SPM > 0.25. Only on station 394 (13 m bottom depth) near the entrance to Kugmallit Bay did the CTD/Rosette sampling from the *CCGS Amundsen* take place sufficiently close to the coast to reach the mineral-dominated water masses. However, the results from barge sampling in August 2009 show that mineral-dominated particle composition was mostly limited to shallow waters less than about 20 m deep near the two Mackenzie River mouths (Fig. 4a). This agrees with past observations suggesting that most mineral-dominated particles transported by the Mackenzie River plume settle to the bottom within the delta or shortly after reaching the shelf where plume speed decreases (Macdonald et al., 1998). For the rest of the shelf and basin surface waters the particle composition in our collected samples showed considerable variability within the organic-dominated and mixed types (Fig. 4). The one exception was, however, the surface sample at station 110 located furthest east in Amundsen Gulf where the POC/SPM was less than 0.0175 (SPM = 3.56 g m^{-3}). Although the possibility of contamination of the sample from station 110 cannot be excluded, the high SPM load could also have been caused by the release of ice-rafted sediments as the ice melted (Bélanger et al., 2013). Deteriorated multiyear ice was observed in the vicinity of the station 110, which could have been the source of minerogenic material.

A notable feature in the particle volume distribution, V(D), was the presence of high concentrations of small particles with diameters D < 1 μm in surface waters and their reduced abundance in subsurface waters (Fig. 4b). The highest increase in the abundance of submicron particles relative to larger particles was found in samples collected furthest to the west along lines 600 and 700 where surface water salinity associated with the river plume was less than 24 PSU. Similar observation also pertains to the surface water sample from station 380 located near the Mackenzie River's Kugmallit Bay channel. The PSD measurements for low salinity, highly turbid samples nearest to the river mouth (stations 390, 394, and 690) were not possible with the Coulter technique. Interestingly, the offshore samples from stations 110 (surface) and 240 (55 m depth) with low POC/SPM ratios were also associated with high concentrations of < 1 μm particles, which is consistent with multiyear ice (suspension freezing) and shelf bottom (resuspension) origins. The volume fraction of < 1 μm particles for the surface water samples at station 240 and the nearby station 235, was 0.12 and 0.18, respectively. At these stations, the near-surface salinity was close to 27.5 PSU. Station 110 stands out among line 100 stations with < 1 μm volume fractions of 0.29 at the surface (salinity of 29.1 PSU) and 0.09 at 60 m depth (31.6 PSU).

In general, the samples for which PSD was measured can be separated based on salinity of the sampled water. The samples with salinity < 30 PSU were collected in the surface layer while the samples with salinity > 30 PSU were collected at a depth of 20 m or deeper. Percentile statistics of V(D) show that small sized particles dominated the particle assemblages within surface waters. The subsurface waters were characterized by larger variability with generally increased contribution of larger particles

Biogeosciences Discuss., https://doi.org/10.5194/bg-2018-261
Manuscript under review for journal Biogeosciences
Discussion started: 21 June 2018

(data not shown). The particle diameters corresponding to the 10th, 50th, and 90th percentiles of V(D), i.e., D_V^{10}, D_V^{50}, and D_V^{90}, respectively, can be summarized as follows: D_V^{10} was within the range 0.71–0.74 μm for salinities < 30 PSU and 0.72–0.98 μm for salinities > 30 PSU; D_V^{50} was in the range 0.78-1.47 μm for salinities < 30 PSU and 1.01–9.45 μm for salinities > 30 PSU; and D_V^{90} was in the range 1.04–15.38 μm for salinities < 30 PSU and 7.96–29.64 μm for salinities > 30 PSU. D_V^{90} showed the smallest differentiation between surface and subsurface waters and a noticeable increase as a function of increasing salinity, which could indicate particle aggregation.

3.2 Relationships between SPM, POC and particulate beam attenuation

The SPM of the samples examined during the MALINA cruise ranged from 0.04 to 140 g m^{-3} with associated POC from 0.007 to 1.5 g m^{-3} (Doxaran et al., 2012). Organic-dominated and mixed particle assemblages were predominant in the portion of the data set obtained from the *CCGS Amundsen* with SPM extending to 5.6 g m^{-3}. The mineral-rich particle assemblages were more common in turbid estuarine waters located close to shore. These waters were sampled using a small barge with an optical package that included a Wetlabs AC-9 meter (Doxaran et al., 2012), but no Wetlabs C-Star 660-nm. The nearest wavelength band on the AC-9 was 676 nm. It thus provided $c_\mathrm{p}(676)$. Note that much higher sediment loads were observed in the region in the past. For example, Carmack and Macdonald (2002, , their Fig. 10) reported on near bottom SPM values of 3000 g m^{-3} due to resuspension of bottom sediments during a storm in September 1987.

Data from all 28 stations with coincident measurements were used in the development of relationships between $c_\mathrm{p}(660)$ and SPM and between $c_\mathrm{p}(660)$ and POC. The particulate beam attenuation coefficient correlated well with both SPM and POC (Fig. 5a, b). Three types of regression analysis for SPM vs. $c_\mathrm{p}(660)$ and POC vs. $c_\mathrm{p}(660)$ were evaluated: (i) a linear fit, (ii) a linear fit to log-transformed data, and (iii) a nonlinear power function fit using the Levenberg-Marquardt optimization algorithm. For the SPM vs. $c_\mathrm{p}(660)$ the differences between the three types of regressions are not significant in terms of the determination coefficient (r^2) which was 0.711 for the linear fit and 0.713 for the other fits. However, the nonlinear power function fit appears to best match the SPM vs. $c_\mathrm{p}(660)$ data. This is supported by reasonably good values of both the root mean square error (RMSE = 0.421 g m^{-3}) and mean normalized bias (MNB = 13.7 %). MNB and RMSE were calculated following equations in Stramski et al. (2008). For comparison, these values were: RMSE = 0.421 g m^{-3} and MNB = 26.0 % for linear fit, and RMSE = 0.457 g m^{-3} and MNB = 11.1 % for linear fit based on log-transformed data. Therefore, we selected the SPM vs. $c_\mathrm{p}(660)$ relationship obtained from nonlinear least squares regression as an algorithm for estimating SPM in [g m^{-3}] from $c_\mathrm{p}(660)$ in [m^{-1}] in the rest of this study:

$$\mathrm{SPM} = 1.933\, c_\mathrm{p}(660)^{0.9364} \tag{2}$$

The regression analysis of POC vs. $c_\mathrm{p}(660)$ data yielded the best results for linear fit to log-transformed data: r^2 = 0.744, RMSE = 0.0449 g m^{-3}, and MNB = 8.72 %. These statistics are, however, only slightly better compared with the other two regression analyses (linear fit: RMSE = 0.0459 g m^{-3} and MNB = 36.16 %, nonlinear power function fit: RMSE = 0.0436 g m^{-3} and MNB = 22.7 %). Hence, for POC we recommend the algorithm obtained from a linear regression to log-transformed

Biogeosciences Discuss., https://doi.org/10.5194/bg-2018-261
Manuscript under review for journal Biogeosciences
Discussion started: 21 June 2018

data:

$$\mathrm{POC} = 0.2071\, c_\mathrm{p}(660)^{0.6842} \tag{3}$$

where POC is in [g m^{-3}] and $c_\mathrm{p}(660)$ in [m^{-1}]. In some instances, for example in biogeochemical modelling studies, the objective may be to estimate light transmission from SPM or POC that has either been measured or is available as model output. The counterparts of Eqs. 2 and 3 are: $c_\mathrm{p}(660)$ = 0.4267 $\mathrm{SPM}^{0.9068}$ and $c_\mathrm{p}(660)$ = 3.088 $\mathrm{POC}^{1.098}$, respectively. The slopes of the best fit lines (with intercepts set to zero) obtained through linear fitting to all pairs of $c_\mathrm{p}(660)$ vs. SPM and $c_\mathrm{p}(660)$ vs. POC data were 0.404 m^2 g^{-1} (r^2 = 0.70) and 3.39 m^2 g^{-1} (r^2 = 0.72), respectively. These slope values represent average SPM-specific and POC-specific particulate beam attenuation coefficients, respectively, for the examined data set. Our average SPM-specific particulate beam attenuation coefficient at 660 nm is consistent with the range 0.2–0.6 m^2 g^{-1} reported by Boss et al. (2009) and Hill et al. (2011) for a 12-m deep coastal site in the North Atlantic Ocean (Martha's Vineyard, MA, USA). Our average POC-specific value is near the middle of the range from 2.31 m^2 g^{-1} at $c_\mathrm{p}(660)$ = 0.45 m^{-1} to 4.10 m^2 g^{-1} at $c_\mathrm{p}(660)$ = 0.07 m^{-1} observed by Stramska and Stramski (2005) in the north polar Atlantic. Jackson et al. (2010) reported beam attenuation vs. SPM and POC correlations for measurements in the Arctic Ocean in 2006–2007, from which we estimate SPM-specific values of 0.34-0.50 m^2 g^{-1} and POC-specific values of 3.4–3.7 m^2 g^{-1} for the $c_\mathrm{p}(660)$ range from 0.07 to 0.45 m^{-1}, respectively. The slopes calculated from our data within this same $c_\mathrm{p}(660)$ range were 0.46 m^2 g^{-1} (r^2 = 0.57) for $c_\mathrm{p}(660)$ vs. SPM and 2.47 m^2 g^{-1} (r^2 = 0.69) for $c_\mathrm{p}(660)$ vs. POC, with the latter being consistent with other datasets (e.g., Cetinić et al., 2012) but notably smaller than the Jackson et al. (2010) value.

The data of SPM used in fitting the relationship of SPM vs. $c_\mathrm{p}(660)$ range from about 0.04 g m^{-3} to 5.6 g m^{-3} (Fig. 5a). This corresponds to $c_\mathrm{p}(660)$ values up to about 3.1 m^{-1}; however, the highest measured $c_\mathrm{p}(660)$ where Wetlabs C-Star measurements were made (but not accompanied by SPM sampling) was 8.8 m^{-1} (at 10 m depth at station 394), which according to Eq. 2 would correspond to SPM of about 14.8 g m^{-3}. For the purpose of examining SPM patterns we use Eq. 2 to extend beyond the maximum measured SPM. A similar non-linear least squares regression analysis that included the highest observed SPM values and corresponding beam attenuation values measured at 676 nm using a Wetlabs AC-9 resulted in a very good fit and a trend line approximating that of the extrapolation of Eq. 2 (Fig. 5c). This supports the assumption that the estimation of SPM from beam attenuation measurements can be reasonably well extended to cover the broader range of values measured with the Wetlabs C-Star, thus being valid from the very clear open ocean to the highly turbid estuarine waters.

The situation is different for the POC vs. $c_\mathrm{p}(676)$ regression. Coincident observations of POC and $c_\mathrm{p}(676)$ reveal a tendency of POC to level off at the very high attenuation values (Fig. 5d). These high $c_\mathrm{p}(676)$ values were all observed from the barge in the shallow estuarine waters of the Mackenzie River mouth (Doxaran et al., 2012). As the particle assemblages within these coastal waters are dominated by mineral particles, a weak relationship between POC and c_p is expected. However, within the POC range up to about 0.45 g m^{-3} and $c_\mathrm{p}(660) \leq 3$ m^{-1} covered by ship-based observations (Fig. 5b), which included only organic-dominated and mixed particle assemblages (POC/SPM $\leq$ 0.06), both $c_\mathrm{p}(660)$ and $c_\mathrm{p}(676)$ are well represented by Eq. 3. This covers the range of $c_\mathrm{p}(660)$ observed along the transect shown in Fig. 1.

Biogeosciences Discuss., https://doi.org/10.5194/bg-2018-261
Manuscript under review for journal Biogeosciences
Discussion started: 21 June 2018

The large range in concentration and composition of suspended particle assemblages (Figs. 4 and 5) collected as a part of the MALINA dataset allowed the determination of empirical relationships for estimating SPM and POC from $c_{\mathrm{p}}(660)$ (Eqs. 2–3) in Canadian Beaufort Sea waters. In the following, SPM distributions in the Canadian Beaufort Sea are investigated by applying the SPM algorithm to $c_{\mathrm{p}}(660)$ data collected during four cruises in the Canadian Beaufort Sea. These cruises include the CASES project in 2004, the ArcticNet cruise in 2007, the IPY–CFL study in 2008, and the MALINA project in August 2009, which altogether cover a wide range of conditions encountered during the open water season in Canadian Beaufort Sea. First, in section 3.3 the environmental forcing and oceanographic conditions during each of these expeditions are described, and then in section 3.4 the observed patterns of the SPM fields are presented and discussed in the context of these conditions. Furthermore, $c_{\mathrm{p}}(660)$ data from four deep casts in Canada Basin collected during the JOIS expedition in September 2009 are examined to show conditions further away from the shelfbreak (Fig. 1).

3.3 Environmental forcing and oceanographic conditions

3.3.1 River discharge and sea ice conditions

The Mackenzie River discharge has large seasonal and interannual variability (e.g., McClelland et al., 2012). Similarly, sea ice concentration on the shelf undergoes large variability (Galley et al., 2008). This is also evident when comparing daily Mackenzie River discharge rates and ice concentrations on the shelf for years 2004, 2007, 2008 and 2009 (Fig. 6). Although the seasonal trend follows a predictable overall pattern, discharge rates during the open water season show significant day-to-day variation, while the timing of landfast ice break-up, wind forcing, and the large-scale circulation of the Beaufort Gyre affect ice concentrations.

The four field expeditions were conducted during different times of the annual cycle with noticeable differences in the Mackenzie River discharge (Fig. 6). The CASES 2004 cross-shelf transects were conducted a few weeks after ice break-up and the freshet. The spring freshet occurred later in 2004 with a sharp peak pulse that reached a higher level than during the other three years. In 2004, the discharge decreased rapidly after the freshet so that the lowest (of the four years) annually averaged discharge occurred. The condition with the highest discharge rates was encountered during the IPY-CFL 2008 transect cross section sampling as late as in early July, when ice concentrations on the shelf were unusually low (around 10 %).

In contrast, the MALINA sampling conditions during August 2009 were characterized by comparatively high (30 %) sea ice concentrations on the shelf. The fresh water released from the melting sea ice competed for surface space with river water, thus affecting plume dynamics and its ability to keep particulate matter in suspension. In contrast to the river waters, sea ice melt waters typically contain little particulate matter and CDOM (e.g., compare Fig. 3b, d, f). However, significant near-surface particle enrichment was observed, which was associated with melt water originating from multi-year ice (Bélanger et al., 2013). During MALINA 2009, numerous multi-year ice floes had drifted into the southeastern Beaufort Sea where they were melting in place (Fig. 7 and Fig. S1 in Supplementary Material).

While the water sampling during the 2004, 2008, and 2009 field experiments occurred during the sea ice melt season, freeze-up had commenced during the ArcticNet sampling in late October 2007. Despite the generally high easterly wind speeds, new

ice formation proceeded rapidly during the second half of October and had formed what appeared as a solid sea ice cover by 22 October along the coastline, largely covering the shelf, and in the offshore pack ice (Fig. 7b). The area around the shelfbreak remained open at the time, a common condition for this flaw lead polynya where delays in the fall freeze-up are often observed (Galley et al., 2008). A solid ice cover along the shore would presumably have reduced direct wind stress on surface waters, however ice motion in offshore waters may instead have contributed to the surface drag and Ekman transport (O'Brien et al., 2011; Spall et al., 2014). Brine release from forming sea ice is further expected to destabilize the water column and enhance vertical mixing.

3.3.2 Wind forcing

Sustained easterly along-shelf winds, particularly when strong, are known to cause shelf surface waters to move offshore through Ekman transport, thereby causing upwelling of deeper nutrient rich water of Pacific-origin onto the shelf (Carmack and Kulikov, 1998; Williams et al., 2006, 2008; Yang, 2009). The high salinity observed during the MALINA expedition in Kugmallit Valley (line 300), Mackenzie Trough (line 600) and near the coast west of 140° W indicated the occurrence of upwelling (Fig. 2). During westerly winds, Ekman transport will cause downwelling flow on the shelf (Dmitrenko et al., 2016). During westerly or weak winds, the river plume tends to flow to the east along the coast of Tuktoyaktuk Peninsula. Relaxation or reversal of either of these winds will cause return flow to occur towards or from the shelf. Furthermore, strong winds promote vertical mixing and may mix shallow shelf waters to the bottom, while freshwater input from either river discharge or ice melt increase vertical stability (e.g., Carmack and Macdonald, 2002). Consequently, three main wind-driven modes of flow affecting SPM patterns on the Mackenzie Shelf can be identified: circulation promoting (i) shelfbreak upwelling or (ii) shelfbreak downwelling, in combination with (iii) degree of vertical mixing of the water column.

The wind vectors reveal a predominance of easterly winds during our study periods in 2004, 2007, 2008 and 2009, with often a southward component resulting in along-shelf wind component (Fig. 8a). High winds are found to be predominantly easterly. The predominance of easterly winds is also a driving force behind the large-scale anticyclonic circulation of the Beaufort Gyre and its ice cover. The occasional reversals of the Beaufort Gyre are related to transient synoptic weather patterns (**?**) that also affect the circulation on the shelf. A notable episode of westerly winds occurred during the fall and winter seasons of 2008–2009 (October and December-January). However, typically the westerly wind events were characterized by low wind speeds.

The wind conditions prior to the four ship-based expeditions (marked by blue circles) are shown in Fig. 8a. During June–July 2004 (CASES) the wind speeds ranged from 2 to 8 m s^{-1} with a variable direction. The sampling during October 2007 ArcticNet expedition was preceded by two weeks of strong easterly along-shelf winds in the excess of 12 m s^{-1}. IPY-CFL sampling (late June and early July 2008) overlapped with CASES in terms of time of year; however, winds were notably different with a month of easterly winds prior to the sampling. The conditions leading up to the MALINA expedition in August 2009 are characterized by <10 m s^{-1} upwelling inducing wind directions in June and most of July, but with a turn to northerly winds during the first part of July, which probably were a contributing factor keeping sea ice on the shelf. Winds during the MALINA expedition were comparatively weak (< 6 m s^{-1}) with variable direction.

Biogeosciences Discuss., https://doi.org/10.5194/bg-2018-261
Manuscript under review for journal Biogeosciences
Discussion started: 21 June 2018

3.3.3 Evidence of upwelling and relaxation

Current speeds and directions were measured at 178 m depth on the CA05 mooring in 2008–2009 (and at 250 m in 2003–2004, and 204 m in 2007–2008) (Fig. 8b). This depth corresponded to the location of the base of the eastward flowing shelfbreak current (Fig. 9a). The currents at this depth on the slope were found to have two distinct modes: (i) along-shelf current that followed the isobaths towards southwest (i.e., $\sim$140°), and (ii) cross-shelf current ($\sim$300°). Interestingly, the shift between the two modes was very brief occurring within only a few hours. Episodes with cross-shelf currents occurred on five occasions in the period between August 2008 and October 2009. In addition, a brief period of change in direction occurred in early August 2009, likely associated with the change in wind direction to southeasterly. The time series collected during 2003–2004 show only a minor cross-shelf flowing event around the beginning of November, while the 2007–2008 time series commenced during what appears to be a strong event in October–November. Each episode with cross-shelf currents, with the exception of November 2003 (the location of the moored instrument was deeper and further east compared to the other year), was associated with increases in salinity and/or temperature, which is an indication of upwelling. All of these events are directly linked to periods with strong easterly along-shelf winds (Fig. 8a) highlighting the likely role of the wind in forcing upwelling. During 2009, the salinity reached up to 34.5 PSU (Fig. 8d), which corresponds to an "effective depth" (see Fig. 3 in Carmack and Kulikov, 1998) of about 300 m indicating a vertical displacement of $\sim$120 m compared to a representative offshore location. Note, however, that the recorded salinity rarely decreased below 33.5 PSU, which in itself corresponds to an "effective depth" of more than 200 m. After the abrupt termination of each upwelling event, temperature and salinity decreased towards pre-upwelling values. Some of the lowest salinity values at 178 m were encountered at the time of the MALINA expedition during August 2009, and likely associated with downwelling return flow.

3.3.4 Geostrophic currents

Geostrophic currents for the cross-shelf sections 100, 200, 300, and 600 were calculated using temperature and salinity data from August 2009 CTD casts (Fig. 9). The reference depth, where the current velocity was assumed to be zero, was selected as 500 m, corresponding to a water mass originating in the Atlantic in which geopotential gradients are small (McPhee, 2013). The sections reveal a westward mean flow of up to 9 cm s^{-1} in the Canada Basin (Fig. 9b, c), which is consistent with the anticyclonic circulation of the Beaufort Gyre. Similarly, currents over the shelf were typically westward with speeds on the order of a few centimeters per second. A notable feature was the presence of an eastward flowing shelfbreak current centered between 100 and 150 m depth (Pickart, 2004). Dmitrenko et al. (2016) presented mooring data collected at lines 200 and 300 shelfbreak locations showing an event of wind-driven shelfbreak current intensification in January 2005 with flow up to 1.2 m s^{-1} during downwelling favorable winds. However, to our knowledge, the current intensification at this location during summer has not been shown in the literature before. The mean easterly flow was around 3 cm s^{-1} (Fig. 9a–c), which is consistent with the observations of Pickart (2004) for the summertime period along the Alaskan Beaufort shelfbreak. The section along line 600 in the Mackenzie Trough captured an anticyclonic mesoscale eddy ($\sim$50 km diameter) which impacted the patterns of $c_{\mathrm{p}}(660)$ and chl-*a* fluorescence (Figs. 3e and 10j).

Biogeosciences Discuss., https://doi.org/10.5194/bg-2018-261
Manuscript under review for journal Biogeosciences
Discussion started: 21 June 2018

3.4 SPM distributions across the continental margin

This section is focused on discussion of SPM fields (Fig. 10), derived from $c_{\mathrm{p}}(660)$ profiles using Eq. 2, along with supporting temperature and salinity fields (Fig. 11). We recall that both Eq. 2 and Eq. 3 are valid for $c_{\mathrm{p}}(660)$ values up to 3.1 m^{-1} (Fig. 5). Thus, this excludes the most mineral-dominated waters on the shelf with SPM over 5.6 g m^{-3} and POC over about 0.5 g m^{-3}. Within the valid range the presented SPM [g m^{-3}] can be converted to POC [g m^{-3}] according to POC $= 0.1279$ SPM$^{0.7307}$, which was derived from the regression analysis of POC vs. SPM data.

3.4.1 Clear waters

SPM ranging between 0.04 and 0.06 g m^{-3} was found in offshore waters in each of the three transect lines measured during June-August (Fig. 10). The low SPM values were especially widespread in August 2009 (MALINA) with wedges of very clear water extending far onto the shelf. The corresponding POC ranged from 0.01 to 0.02 g m^{-3}. The extension of clear waters onto the shelf as a wedge between the surface plume and the turbid near bottom layer has been described by Carmack et al. (1989). It appears that neither particle settling from the surface plume nor the resuspension of bottom sediments were sufficient in August 2009 to increase these clear-water values of $c_{\mathrm{p}}(660)$ above those found in deep basin surface waters. The landward extension of the clear-water layer was particularly noticeable on line 600 (Fig. 10j) which corresponds with the Mackenzie Trough (a submarine canyon), the main river channel and the most distinct surface plume feature of the transects. The conditions during MALINA differed from the previous years particularly in terms of sea ice coverage (Fig. 7b). The break-up of the landfast ice on the shelf occurred late and ice floes were not readily transported away from the shelf due to the northerly and later weak winds. Furthermore, multiyear ice extended further south compared to previous years considered in this study (Fig. 7). As surface salinity remained low for the length of the line 300 (Fig. 11h), the melt water from this ice appears to have influenced the low SPM levels in the shelf waters by increasing the stratification that reduced mixing and by hindering the spread of the particle-rich river plume.

3.4.2 Effect of ice melt on SPM distribution

Comparatively high levels of SPM were found along line 300 (Kugmallit Valley) near the shelf bottom in August 2009 with particularly high values extending across the shelf (Fig. 10h). Such SPM patterns are indicative of downwelling return flow from the shelf after upwelling-inducing wind conditions relaxed. These near-bottom concentrations match those observed during the fall 2007 (Fig. 10f) under high winds (Fig. 8) and brine release from forming ice (Fig. 7) and generally higher salinity shelf waters (Figs. 11b, f). The presence of sea ice and its meltwater on the shelf during August 2009, as seen from the low surface temperatures and salinities at $\sim$70.9° N (Fig. 11h), can explain the containment of the spreading of the plume along line 300 (Fig. 10h). High particle settling rates from a slow moving or stagnant river plume may in turn explain the high near bottom SPM which then could be transported along the shelf bottom with the return flow of the upwelled waters.

A contrasting situation is provided by the conditions observed along line 300 during June-July 2008 (IPY-CFL study) (Figs. 10g and 11g). During the IPY-CFL, ice coverage on the shelf was low (Fig. 6b) and upwelling-inducing winds prevailed

throughout June and early July (Fig. 8). Consequently, the two compared SPM sections along line 300 differed markedly (Fig. 10g, h). As seen in Fig. 10g, in 2008 the turbid surface river plume spread northward past the shelfbreak. This buoyancy-driven flow was likely enabled by the absence of ice melt water. The near-bottom turbidity was low likely owing to conditions resulting from the notable upwelling event evidenced by the high salinity of the shelf bottom water and the extent of the turbid surface plume (see Fig. 11g).

3.4.3 River plume variability

Wind-forcing largely controls the flow direction of the Mackenzie River plume. Due to the size and shape of the Mackenzie Shelf, the most likely direction for the Mackenzie River plume to spread significant distances past the shelfbreak is to the northwest (Doxaran et al., 2012). The MALINA sampling occurred during a time of transition from a northwestward plume towards a Coriolis-forced right turning plume flowing eastward along the coast. Plumes of both directions are visible in MODIS satellite images for the period of the MALINA expedition (Doxaran et al., 2012; Forest et al., 2013). The sampling along lines 600 and 700 was conducted during the first half of August 2009, following a two-week period of easterly winds (Fig. 8a). By 26 July, the plume was clearly seen extending out past the tip of Cape Bathurst. By mid-August only very weak features remained from the northwestward plume. Notably, both river discharge and ice concentrations on the shelf were reduced by half during the period of one month (Fig. 6).

Figures 10i, j, and 11i, j show the river plume extending northwest along the Mackenzie Trough (line 600). The Mackenzie River plume occupied an about 15 m thick layer at the surface both in July 2004 and August 2009. A sharp decrease in SPM was found immediately below this layer. The surface plumes were accompanied by low salinities and, at least for 2009, high CDOM fluorescence (Fig. 3f) indicating a riverine origin (Matsuoka et al., 2012). Interestingly, particle concentrations differed markedly for the two years compared. In 2004 high levels of SPM extended the full length of the transect with values reaching 4 g m^{-3} as far as 70° N. In contrast, in 2009 the SPM values observed in the plume were only about 10 % of the 2004 values but still distinctly noticeable because the plume overlaid a layer of very clear water. Also, the waters beneath the river plume in 2004 were significantly more turbid compared to 2009, probably due to settling of particles from the plume.

Although the timing of the transect measurements in 2004 and 2009 was a month apart, overall conditions on the shelf were not markedly different. Easterly winds were weak in both cases (Fig. 8), ice coverage on the shelf was 30–40 %, and the river discharge was ∼13,000-14,000 m^3 s^{-1} during both years (Fig. 6). Moreover, the cross sections along lines 100 and 300 (Figs. 10 and 11) show very similar features and particle concentrations during the two years. The differences between the two situations can be attributed to the seasonal timing. The 2004 transects were measured in early July soon after the break-up of the landfast sea ice cover and the surge of backed-up river waters across the delta and estuary. In contrast, the 2009 measurements were conducted much later in the season after landfast ice break-up. Consequently, in 2004 the surface plume was likely conditioned by a greater initial SPM discharge at the river mouth and by a higher momentum compared to 2009 so that it was capable of keeping more particles in suspension for a longer distance, including larger-sized particles if present. MODIS imagery of sea-surface temperature for 2 July 2004 (Fig. S3 in Supplementary Material) highlights this river plume inertia.

Biogeosciences Discuss., https://doi.org/10.5194/bg-2018-261
Manuscript under review for journal Biogeosciences
Discussion started: 21 June 2018

3.4.4 Freeze-up conditions

Measurements in October 2007 showed a well-mixed upper layer of ∼30 m with the highest observed salinities and lowest temperatures on the shelf (Figs. 11b, f). These high salinities were caused by upwelling that was forced by strong easterly winds (Fig. 8; see also Tremblay et al., 2011), but were likely also related to new ice formation that was taking place in shelf waters (Figs. 6 and 7). To illustrate this point, a 30-PSU salinity of a 20-m deep water column would increase by only 0.3 PSU from salt rejected by the formation of 0.3 m thick sea ice (World Meteorological Organization classification for the maximum thickness of the young ice type). Therefore, it is unlikely that sea ice formation alone could account for the observed high salinity.

Similarly to the physical properties, the SPM estimates from $c_{\mathrm{p}}(660)$ were well-mixed in shelf waters with estimated values reaching 4 g m^{-3} (Fig. 10b, f). Despite the overall higher salinity of the water column in October compared to summer, a halocline was present at 30 m depth (Fig. 11f) beneath which high SPM levels extended towards the shelfbreak. This is an indication of cross-shelf transport of sediment near the bottom. The importance of the release of high-density brine from sea ice formation to particle transport across the Canadian Beaufort shelfbreak was discussed by Forest et al. (2007).

In October 2007 a 40–50 m thick layer of the upper water column with SPM in the range 0.40–0.55 g m^{-3} extended the full length of the still ice-free line 100 (Fig. 10b). These are the highest values seen for surface waters within the Amundsen Gulf in our study. The source of these particles in the Amundsen Gulf is difficult to trace. Winds were sufficiently strong to cause resuspension of SPM on the shelf and other nearby coastal areas. However, the wind direction was easterly (Fig. 8) such that surface waters on the Mackenzie shelf and in Amundsen Gulf flowed mainly northwest, i.e., away from Amundsen Gulf (measured with acoustic current profiler on mooring CA05; data not shown). In freezing waters the $c_{\mathrm{p}}(660)$ signal could have been affected by the formation of frazil ice (small ice crystal particles). However, in this case this was not likely to happen because the surface layer along line 100 remained 0.5–1.5 °C above the freezing point even though ice was forming on the shelf and along the coast (Fig. 7). Tremblay et al. (2011) reported on the upwelling of nutrients to reach the highest concentration of nitrate (16.8 μM) ever observed in the region on the shelf northwest of Cape Bathurst, which caused an increase in primary production. These high nitrate values did not extend far past the shelfbreak and remained low across Amundsen Gulf. Although, chl-*a* fluorescence data for the surface waters indicated the elevated concentrations of phytoplankton (Tremblay et al., 2011), it is not possible to conclude that phytoplankton concentrations were sufficient to explain the high $c_{\mathrm{p}}(660)$.

3.4.5 Implications to primary production

The high $c_{\mathrm{p}}(660)$ values near the shelf seafloor in August 2009 were accompanied by a strong chl-*a* fluorescence signal that extended from the shelf into the Canada Basin as a subsurface chl-*a* maximum (SCM) layer (Fig. 3). The productivity of the SCM is generally proportional to concentration of chl-*a* and limited by light and nutrient availability (Martin et al., 2010). SPM distribution may be of importance for the formation and maintenance of the SCM as illustrated by the two following examples from our observations.

First, the patterns of $c_{\mathrm{p}}(660)$ and chl-*a* fluorescence suggest that biological production on the shelf bottom was enhanced by the upwelled nutrient-rich waters and, at the time of our measurements, biogenic material was being transported seaward in an intermediate nepheloid layer across the shelfbreak at 50–70 m depth (Figs. 3 and 10; Tremblay et al., 2011). The shelf circulation at play makes it conceivable that the transport of biogenic material produced on the shelf, including resuspension of settled particles originating from an earlier bloom (e.g. ice algae), could potentially influence the formation and maintenance of the SCM in the off-shelf region. Thus, the study of shelf-basin exchange processes leading to the subsurface transport of nutrients and biogenic material may be of biological importance to improve the understanding of pelagic-benthic coupling in the region.

Second, the subsurface light availability in the Beaufort Sea and Amundsen Gulf is largely governed by the seasonal cycle and the presence of sea ice. Tremblay et al. (2011) discussed these conditions, as well as nutrient dynamics, leading up to the high biological productivity observed in the Amundsen Gulf during summer 2008. Our observations indicate that the SCM may also be influenced by the optical clarity of the surface water layer. For example, July 2008 (Fig. 10c) displayed higher SPM in the SCM centered at the 31.5 PSU isohaline (50 m depth) compared to June 2004 and August 2009 (Fig. 10a, d). This indicates that higher levels of solar radiation reached the SCM such that phytoplankton growth could reach a higher biomass.

Whereas ice free and comparatively clear surface waters were present in 2008 (Fig. 10c), turbid (i.e., high $c_{\mathrm{p}}(660)$ and SPM) surface layers extended across Amundsen Gulf in 2004, 2007 and 2009 (Fig. 10a, b, d), and the surface was partially ice covered in June 2004 (Fig. 7a). Time of year and consequent differences in river discharge and ice conditions are naturally expected to influence the size of the Mackenzie River plume. The temperature and salinity fields, however, show only modest differences between conditions in 2004, 2008 and 2009 (Fig. 11a, c, d). This suggests that the fresh and turbid surface layers present in 2009 were caused by the spreading of fresh shelf waters affected by the Mackenzie River, while the equally fresh but clear layer in 2008 was associated with sea ice melt water. The difference in conditions between the years may thus be explained by the presence or absence of sea ice, and generally by the history of wind forcing, and how these two factors affect the spreading of the river plume.

3.4.6 Nepheloid layers on the slope and beyond

Figure 10 reveals a ubiquitous presence of numerous subsurface nepheloid layers extending from the Beaufort Sea continental slope. These nepheloid layers are produced primarily by resuspension of bottom sediments settled onto the shelf or slope, and provide evidence for the transport of suspended particles and water away from the shelf. It is important to differentiate these layers from the mainly locally formed subsurface chl-*a* maximum (SCM) layer that is commonly present in the Canadian Beaufort Sea (Martin et al., 2010; Tremblay et al., 2011). As the SCM seems to intersect with the shelf bottom (Fig. 3), the presence of relatively high chl-*a* concentrations within subsurface nepheloid layers may however conceal the presence of minerogenic particles at the same depth.

On line 600, two subsurface nepheloid layers (in addition to the surface river plume) extending from the shelf at depths of 100–130 m and 200–250 m, were observed in 2004 and 2009 (Fig. 10i, j). These two layers appeared to form near where the 33.1 PSU isohalines intersected the shelf seafloor and immediately above and below a slightly less sloping section of the

Biogeosciences Discuss., https://doi.org/10.5194/bg-2018-261
Manuscript under review for journal Biogeosciences
Discussion started: 21 June 2018

Mackenzie Trough bottom (Fig. 11i, j). However, only the upper layer was accompanied by relatively high chl-*a* fluorescence (Fig. 3e). The depths of 100 m and greater are beneath the euphotic layer rendering primary production negligible. Thus, these chl-*a* containing particles likely represent transported particles that originated in shallower shelf waters.

Numerous intermediate nepheloid layers (INLs) are seen in the upper 500 m of the water column throughout the Amundsen Gulf (Figs. 10a-d) and extending into Canada Basin (Figs. 10e-j). The cast-to-cast variability in the depth location of these INLs is large (Fig. 12) making it difficult to trace the shelf/slope origin of the INLs in this dynamic system. Generally, the SPM of INLs in offshore waters was an order of magnitude smaller than in the benthic nepheloid layer (BNL) on shelf and particle concentrations decreased with distance from the shelf.

Beneath 500 m depth, the vertical profiles of SPM still showed numerous inversions (Fig. 12). Generally, however, the particle concentration at specific depths decreased as bottom depth increased as it also relates to the distance from the shelfbreak. This decrease is approximately exponential with distance from the shelfbreak. In waters less than 3000 m deep located on the continental slope and rise, the SPM began to increase from about the mid depth of the water column which had the clearest waters. The thickness of these BNLs ranged from ∼200 m (station 340) to over 1000 m (Fig. 12). Past the 3000 m bottom depth, BNLs were essentially absent with the clearest waters found close to the bottom as may also be the case for the Canada Basin abyssal plain (Hunkins et al., 1969). Near-bottom SPM values based on $c_{\mathrm{p}}(660)$ were $\sim 2\times10^{-3}$ g m-3 at the station CB-27, and decreased to $\sim 1\times10^{-3}$ g m^{-3} at 3500 m at CB-21 (74.0042° N, 139.8699° W, i.e., 113 km north of CB-27) on 9 October. After detaching from the BNL on the slope, INLs were advected along isopycnal surfaces. With distance, INLs became thinner with lower SPM owing to lateral spreading to cover larger areas, mixing at layer boundaries, and settling of particles.

It is thus of interest to investigate in more detail two obvious INLs seen in Fig. 12a. Station 530 showed an INL at 1200 m depth with SPM of ∼0.030 g m^{-3}. SPM in the overlying water was 0.021 g m^{-3}. It is clear that the INL must have been detached and advected from the bottom layers on the slope (perhaps near to adjacent stations 550 or 440 with a near-bottom SPM of 0.050 g m^{-3} at 1050–1100 m). Interestingly, station CB-27 located at 73° N showed a similar INL with the SPM maximum of 6.9×10^{-3} g m^{-3} at 1170 m where the potential density anomaly, σ_θ, was 28.032 kg m^{-3}. However, neither CB-23 nor CB-31 located to the east had INLs at that isopycnal. Over the distance of 240 km separating the stations 530 and CB-27, the SPM decreased by about 0.023 g m^{-3}, which corresponds to about 1×10^{-4} g m^{-3} km^{-1}.

A notable INL at stations CB-23, CB-27, and CB-21 was spreading in the layer immediately below the isopycnal surface where the potential density anomaly σ_θ reached 28.096 kg m^{-3} or the salinity reached 34.956 (Fig. 12). The depth where this occurred varied between the stations. Beneath this interface the potential temperature was uniform with depth, thereby marking a transition to the adiabatic Canada Basin bottom water layer (e.g., Timmermans et al., 2003). Assuming that the particles in the INL were from the bottom layer of CB-31 (1920 m depth with σ_θ = 28.093 kg m^{-3}), then the transport of particles from the bottom of station CB-31 to the INL at station CB-23 requires a 560 m increase in depth over a 100 km distance, which equals a sinking rate of 5.6 m km^{-1}. Such transport of particles crosses isopycnal surfaces, suggesting the predominant role of particle settling in addition to advective transport. Furthermore, following the BNL to station 330 from CB-31, the BNL depth increased by 900 m over the distance of 88 km such that the descent rate was 10.2 m km^{-1}. This decrease in the rate of sinking

with distance from the slope may illustrate the process by which the larger/heavier particles sink faster, or are broken down by biological processes, and are gradually removed from the nepheloid layer until only smaller particles remain in suspension. Some smaller sized particles may additionally have detached from the BNL forming the numerous INLs as observed, for example, at station CB-31 at depths between 1100 and 1900 m.

The maximum SPM within the INL at station CB-23 was 0.0126 g m^{-3} at 2470 m depth. At CB-27 the maximum was 8.2×10^{-3} g m^{-3} at 2600 m (Fig. 12). The SPM levels above the INLs (with σ_θ = 28.095) were 0.010 and 0.027 g m^{-3}, respectively. Given that the INL depth increased by 130 m over the 128 km distance that separated the two stations, the INL descent rate was about 1 m km^{-3}. A thinner (50 m thick) and weaker INL with a maximum SPM of 3.2×10^{-3} g m^{-3} at 2656 m was observed at CB-21 (Fig. 12d). The INL descent rate over 113 km distance between CB-27 and CB-21 was about 0.5 m km^{-1}. Because the maximum SPM at these INLs occurred at the same σ_θ, this descent of the INLs was determined by the water mass structure, however, the decrease of SPM within the maxima reflect processes such as spreading, settling, aggregation, scavenging, and mixing of particulate matter. The SPM in the INL was found to decrease linearly with the square root of distance from the shelf while background SPM decreased exponentially with distance. A correlation analysis based on data from station 330 and the four stations from CB-31 through CB-21, showed a linear decrease in SPM at the INL maxima as a function of the depth location of the maximum, z_{peak} with the best fit equation SPM [g m^{-3}] = -3.88×10^{-5} z_{peak} + 0.107 (r^2=0.99). Interestingly, both the depth and the magnitude of the SPM maximum were found to increase or decrease linearly with the square root of the distance from the shelfbreak with slopes of 92.3 m $km^{-1/2}$ (r^2=0.97) and -3.6×10^{-3} g m^{-3} $km^{-1/2}$ (r^2=0.97), respectively.

4 Summary and Conclusions

The data collected in the Beaufort Sea during the MALINA field campaign in 2009 enabled the development of relationships for estimating SPM and POC from measurements of optical beam attenuation coefficient. These relationships provided, in turn, a means for obtaining a comprehensive view of particle concentration fields and characteristics covering the full expanse of the Canadian Beaufort Sea continental margin on the basis of optical data collected during several expeditions in this region. Our analysis revealed temporal and spatial variations in particle concentration and dynamics which could be attributed to (i) discharge of Mackenzie River, (ii) ice coverage and thermodynamics, and (iii) wind forcing. These three factors affect the advection of the river plume and the overall circulation on the shelf. As a result there are three modes of particle transport on the shelf; (1) within a buoyant surface plume, (2) resuspended particles within a benthic nepheloid layer (BNL), and (3) within a mixed water column during high wind speeds (> 12 m s^{-1}). SPM on the shelf exceeds 1 g m^{-3} in each of these cases. A clear water layer was typically found in mid-layers on the shelf. Similar features were also noted by Carmack et al. (1989).

We found that the buoyant sea ice melt water competed for space with the river plume, and in contrast contained little particulate matter (and CDOM; Fig. 3), which had a significant effect on SPM distributions within the surface layer. When ice melt water was present on the shelf during years with high ice coverage (Fig. 11), it appeared to restrict the expansion of the surface river plume, and cross-shelfbreak transport of particles was consequently found to occur mainly along the shelf bottom

in a BNL (Fig. 10). This was a consequence of two factors: (i) the reduction in plume buoyancy driving force by the sea ice melt water layer such that more particles carried by a slower moving or stagnant plume were settled to the bottom, and (ii) weak or westerly winds that allowed sea ice and melt water to remain on the shelf and caused downwelling return flow (after relaxation of wind-induced upwelling) that could transport particles in the BNL.

The wind-driven upwelling signal was clearly present in the current meter record at the base of the Pacific Water layer at 180–200 m for mooring CA05 (Fig. 8b) located on the continental slope (Fig. 1) at a depth corresponded to an eastward flowing shelfbreak jet (Fig. 9). At the 180-200 m depth, the currents were seen to follow isobaths during quiescent conditions, but then switched to moving cross shelf during strong upwelling favorable winds (Fig. 8a). Interestingly, there appeared to be two very distinct modes of flow at this depth along the slope. In 2009, the salinity at 178 m reached 34.5 during the upwelling events (Fig. 8c), which corresponds to an effective depth of about 300 m (Carmack and Kulikov, 1998). However, in all cross-shelf transects shown in Fig. 11, salinities of at least 32.3 PSU were found on the shelf at 60–80 m depth. This salinity corresponded to the transition between Pacific Summer Water and Winter Water, which is typically found at 100 m depth in the Canada Basin (e.g., Carmack et al., 1989). The salinity on the shelf was higher than in corresponding Canada Basin waters at all times and all observed sections. Thus, a modest 20–40 m of (depth equivalent) upwelling onto the shelf may represent a steady state condition linked to the generally easterly wind and anticyclonic circulation of the Beaufort Gyre.

The presence of the SCM layer (Martin et al., 2010) at the base of the Pacific Summer Water mass was a consistent feature in the southern Beaufort Sea but was also observed to intersect with the BNL on the shelf (Fig. 3). Apart from the SCM, the depth locations and particle concentrations of INLs were found to be highly variable and numerous in top 500 m of the water column, highlighting the complex conditions responsible for their formation. The high SPM seen on the shelf did not extend far past the shelfbreak except in a westward flowing river plume (Fig. 10; see also Fig. S2 in Supplementary Material). Thus, subsurface sediment transport beyond the shelfbreak must occur in a near bottom BNL which detaches into INLs at specific depths as determined by physical processes and particle characteristics. Further research is required to explore this observation in detail. Past the shelfbreak, the SPM at specific depths generally decreased with distance from the shelfbreak and with increasing depth. The $c_{\mathrm{p}}(660)$ profiles in Canada Basin waters agree with the two types of profiles described in Hunkins et al. (1969), first, in waters with bottom depths less than about 3000 m the SPM had minimum values roughly at mid-depths of the water column and then increased towards the bottom forming a c-shaped profile, and second, in waters exceeding the 3000 m depth the SPM reached minimum values near the bottom. The deepest INL (below which no INLs were seen) extending to the Canada Basin abyssal plain was observed at the 2500–2600 m depth at the top of the adiabatic Canada Basin bottom water layer (Timmermans et al., 2003).

As the Arctic continues to warm, the open water season is expected to become increasingly longer and the extent of multiyear ice further decline (Stroeve et al., 2014). The reduction in ice coverage in the Beaufort Sea implies an increase in SPM dynamics on the continental margin due to the associated changes in wind forcing and river discharge (Carmack et al., 2006). Greater wind and wave forcing on open waters is expected to increase particle concentrations on the shelf. However, the presence of both clear intermediate waters and highly turbid bottom waters observed on the shelf in this study highlighted interesting linkages to the effect of sea ice on river water and particle transport on the shelf, which need further study. The processes that operate within

subsurface layers and ice-covered waters cannot be deciphered through satellite remote sensing, so their quantification requires in-situ monitoring. Optical beam transmission is a simple yet efficient tool for mapping SPM distributions. The relationship between SPM and $c_{\mathrm{p}}(660)$ developed in this study can be applied to past and future transmissometer observations to monitor changes to SPM. Vertical measurements reaching all the way to the seafloor would be very beneficial when attempting to determine lateral SPM transport. This is typically not done due to the risk to the instruments. Furthermore, ongoing research that considers current speeds together with particle size distributions are needed in order to shed more light on particle transport and settling processes across the Beaufort Sea shelf, slope and rise which are experiencing considerable change in response to river discharge, sea ice coverage, and wind forcing.

Data availability. All data used in this study are available in the following online data bases: Polar Data Catalogue, Water Survey of Canada (Environment Canada), Canadian Ice Service (Environment Canada), National Centers for Environmental Prediction (NCEP), and the French national IMBER/SOLAS data base.

Author contributions. JKE drafted the manuscript, analyzed the data and prepared the figures. JKE and DD collected and analysed the SPM and POC data, while RR conducted the particle size distribution sampling. All coauthors contributed to writing the manuscript.

Competing interests. The authors declare that they have no conflict of interest.

Acknowledgements. This study was conducted as part of the MALINA Scientific Program funded by ANR (Agence Nationale de la Recherche), INSU-CNRS (Institut National des Sciences de l'Univers – Centre National de la Recherche Scientifique), CNES (Centre National d'Etudes Spatiales), ESA (European Space Agency), and the ArcticNet Canadian Network of Centres of Excellence. Additional funding for JKE, RAR, and DS was provided by the US National Aeronautics and Space Administration (Grant NNX07AR20G). JKE is funded by the Natural Sciences and Engineering Research Council of Canada (NSERC) Discovery Grant program. We thank the National Aeronautics and Space Administration (NASA), National Centers for Environmental Prediction (NCEP), and Environment Canada for providing free access to data. We thank all participants on the CASES, ArcticNet, IPY-CFL and MALINA cruises for their help, and in particular all of the crew members on *CCGS Amundsen*.

References

Asplin, M. G., Galley, R., Barber, D. G., and Prinsenberg, S.: Fracture of summer perennial sea ice by ocean swell as a result of Arctic storms, J. Geophys. Res., 117, C06025, doi:10.1029/2011JC007221, 2012.

Babin, M., Stramski, D., Ferrari, G. M., Claustre, H., Bricaud, A., Obolensky, G., and Hoepffner, N.: Variations in the light absorption coefficients of phytoplankton, nonalgal particles, and dissolved organic matter in coastal waters around Europe, J. Geophys. Res., 108 (C7), 3211, doi:10.1029/2001JC000882, 2003a.

Babin, M., Morel, A., Fournier-Sicre, V., Fell, F., and Stramski, D.: Light scattering properties of marine particles in coastal and open ocean waters as related to the particle mass concentration, Limnol. Oceanogr., 48(2), 843–859, 2003b.

Barber, D. G., Asplin, M. G., Gratton, Y., Lukovich, J. V., Galley, R. J., Raddatz, R. L., and Leitch, D.: The International polar year (IPY) circumpolar flaw lead (CFL) system study: Overview and the physical system, Atmos.-Ocean, 48(4), 225–243, doi:10.3137/OC317.2010, 2010.

Bélanger, S., Cizmeli, S. A., Ehn, J., Matsuoka, A., Doxaran, D., Hooker, S., and Babin, M.: Light absorption and partitioning in Arctic Ocean surface waters: impact of multiyear ice melting, Biogeosciences, 10, 6433–6452, doi:10.5194/bg-10-6433-2013, 2013.

Bishop, J. K. B.: The correction and suspended mass calibration of Sea Tech transmissometer data, Deep-Sea Res., 33, 121–134, 1986.

Bishop, J. K. B: Transmissometer measurement of POC, Deep-Sea Res., I 46, 353–369, 1999.

Boss, E., Slade, W., and Hill, P.: Effect of particulate aggregation in aquatic environments on the beam attenuation and its utility as a proxy for particulate mass, Opt. Express, 17(11), 9408–9420, doi:10.1364/OE.17.009408, 2009.

Bricaud, A., Morel, A., and Prieur, L.: Absorption by dissolved organic matter of the sea (yellow substance) in the UV and visible domains, Limnol. Oceanogr., 26, 43–53, doi:10.4319/lo.1981.26.1.0043, 1981.

Bunt, J. A. C., Larcombe, P., and Jago, C. F.: Quantifying the response of optical backscatter devices and transmissometers to variations in suspended particulate matter, Cont. Shelf Res., 19(9), 1199–1220, doi:10.1016/S0278-4343(99)00018-7, 1999.

Carmack, E. C., Macdonald, R. W., and Papadakis, J. E.: Water mass structure and boundaries in the Mackenzie shelf estuary, J. Geophys. Res., 94, 18043–18055, 1989.

Carmack, E., Barber, D., Christensen, J., Macdonald, R., Rudels, B., and Sakshaug, E.: Climate variability and physical forcing of the food webs and the carbon budget on panarctic shelves, Prog. Oceanogr., 71, 145–181, doi:10.1016/j.pocean.2006.10.005, 2006.

Carmack, E. C., and Kulikov, E. A.: Wind-forced upwelling and internal Kelvin wave generation in Mackenzie Canyon, Beaufort Sea, J. Geophys. Res., 103, 18447–18458, 1998.

Carmack, E. C., and Macdonald, R. W.: Oceanography of the Canadian shelf of the Beaufort Sea: A setting for marine life, Arctic, 55 (Supp. 1), 29–45, 2002.

Cetinić, I., Perry, M. J., Briggs, N. T., Kallin, E., D'Asaro, E. A., and Lee, C. M.: Particulate organic carbon and inherent optical properties during 2008 North Atlantic Bloom Experiment, J. Geophys. Res., 117, C06028, doi:10.1029/2011JC007771, 2012.

Doxaran, D., Ehn, J., Bélanger, S., Matsuoka, A., Hooker S., and Babin, M.: Optical characterisation of suspended particles in the Mackenzie River plume (Canadian Arctic Ocean) and implications for ocean colour remote sensing, Biogeosciences, 9, 3213–3229, doi:10.5194/bg-9-3213-2012, 2012.

Dmitrenko, I. A., Kirillov, S. A., Forest, A., Gratton, Y., Volkov, D. L., Williams, W. J., Lukovich, J. V., Belanger, C., and Barber, D. G.: Shelfbreak current over the Canadian Beaufort Sea continental slope: Wind-driven events in January 2005, J. Geophys. Res., 121, doi:10.1002/ 2015JC011514, 2016.

Forest, A., Sampei, M., Hattori, H., Makabe, R., Sasaki, H., Fukuchi, M., Wassmann, P., and Fortier, L.: Particulate organic carbon fluxes on the slope of the Mackenzie Shelf (Beaufort Sea): Physical and biological forcing of shelf-basin exchanges, J. Mar. Sys., 68, 39–54, doi:10.1016/j.jmarsys.2006.10.008, 2007.

Forest, A., Bélanger, S., Sampei, M., Sasaki, H., Lalande, C., and Fortier, L.: Three-year assessment of particulate organic carbon fluxes in Amundsen Gulf (Beaufort Sea): Satellite observations and sediment trap measurements, Deep-Sea Res. I, 57, 125–142, doi:10.1016/j.dsr.2009.10.002, 2010.

Forest A., Babin, M., Stemmann, L., Picheral, M., Sampei, M., Fortier, L., Gratton, Y., Bélanger, S., Devred, E., Sahlin, J., Doxaran, D., Joux, F., Ortega-Retuerta, E., Jeffrey, W. H., Martín, J., Gasser, B., Miquel, J. C.: Ecosystem function and particle flux dynamics across the Mackenzie Shelf (Beaufort Sea, Arctic Ocean): an integrative analysis of spatial variability and biophysical forcings, Biogeosciences, 10, 2833–2866, 2013.

Galley, R. J., Key, E., Barber, D. G., Hwang, B. J., and Ehn, J. K.: Spatial and temporal variability of sea ice in the southern Beaufort Sea and Amundsen Gulf: 1980–2004, J. Geophys. Res., 113, C05S95, doi:10.1029/2007JC004553, 2008.

Gardner, W. D., Mishonov, A. V., and Richardson, M. J.: Global POC concentrations from in-situ and satellite data, Deep-Sea Res. II, 53, 718–740, doi:10.1016/j.dsr2.2006.01.029, 2006.

Guay, C. K. H., and Bishop, J. K. B.: A rapid birefringence method for measuring suspended CaCO3 concentrations in seawater, Deep-Sea Res. I, 49, 197–210, 2002.

Hill, P. S.,Boss, E., Newgard, J. P., Law, B. A., and Milligan, T. G.: Observations of the sensitivity of beam attenuation to particle size in a coastal bottom boundary layer, J. Geophys. Res., 116, C02023, doi:10.1029/2010JC006539, 2011.

Honjo, S., Krishfield, R. A., Eglinton, T. I., Manganini, S. J., Kemp, J. N., Doherty, K., Hwang, J., McKee, T. K., and Takizawa, T.: Biological pump processes in the cryopelagic and hemipelagic Arctic Ocean: Canada Basin and Chukchi Rise, Prog. Oceanogr., 85, 137–170, doi:10.1016/j.pocean.2010.02.009, 2010.

Hunkins, K., Thorndike, E. M., and Mathieu, G.: Nepheloid layers in the Arctic Ocean, J. Geophys. Res., 74(28), 6995–7008, 1969.

Ingram, R. G., Williams, W. J., van Hardenberg, B., Dawe, J. t., and Carmack, E. C.: Seasonal circulation over the Canadian Beaufort Shelf, in: On Thin Ice: a synthesis of the Canadian Arctic Shelf Exchange Study (CASES), Aboriginal Issues Press, Winnipeg, Manitoba, Canada, 14–35, 2008.

Jackson, J. M., Allen, S. E., Carmack, E. C., and McLaughlin, F. A.: Suspended particles in the Canada Basin from optical and bottle data, 2003–2008, Ocean Sci., 6, 799–813, doi:10.5194/os-6-799-2010, 2010.

Kirillov, S., Dmitrenko, I., Tremblay, B., Gratton, Y., Barber, D., and Rysgaard, S.: Upwelling of Atlantic water along the Canadian Beaufort Sea continental slope: Favorable atmospheric conditions and seasonal and interannual variations, J. Climate, 29, 4509–4523, doi.org/10.1175/JCLI-D-15-0804.1, 2016.

Kitchen, J. C., Zaneveld, J. R. V., and Pak, H.: Effect of particle size distribution and chlorophyll content on beam attenuation spectra, Appl. Opt., 21, 3913–3918, doi:10.1364/AO.21.003913, 1982.

Knap, A., Michaels, A., Close, A., Ducklow, H., and Dickson, A. (Eds.): Protocols for the Joint Global Ocean Flux Study (JGOFS) Core Measurements, JGOFS Report Nr. 19, vi+170 pp., Reprint of the IOC Manuals and Guides No. 29, UNESCO, 1996.

Macdonald, R. W., Solomon, S. M., Cranston, R. E., Welch, H. E., Yunker, M. B., and Gobeil, C.: A sediment and organic carbon budget for the Canadian Beaufort shelf, Marine Geology, 144(4), 255–273, doi:10.1016/S0025-3227(97)00106-0, 1998.

Martin, J., Tremblay, J.-E., Gagnon, J., Tremblay, G., Lapoussière, A., Jose, C., Poulin, M., Gosselin, M., Gratton, Y. and Michel, C.: Prevalence, structure and properties of subsurface chlorophyll maxima in Canadian Arctic waters, Mar. Ecol. Prog. Ser., 412, 69–84, doi: 10.3354/meps08666, 2010.

Matsuoka, A., Bricaud, A., Benner, R., Para, J., Sempéré, R., Prieur, L., Bélanger, S., and Babin, M.: Tracking the transport of colored dissolved organic matter in the Southern Beaufort Sea: relationship with hydrographic characteristics, Biogeosciences, 9, 925–940, doi:10.5194/bg-9-925-2012, 2012.

McClelland, J. W., Holmes, R. M., Dunton, K. H., and Macdonald, R. W.: The Arctic Ocean Estuary, Estuar. Coast., 35, 353–368, doi:10.1007/s12237-010-9357-3, 2012.

McPhee, M. G.: Intensification of Geostrophic Currents in the Canada Basin, Arctic Ocean, J. Clim., 26, 3130–3138, doi:10.1175/JCLI-D-12-00289.1, 2013.

Moore, G. W. K.: Decadal variability and a recent amplification of the summer Beaufort Sea High, Geophys. Res. Lett., 39, L10807, doi:10.1029/2012GL051570, 2012.

Morel, A. and Bricaud, A.: Inherent optical properties of algal cells, including picoplankton: Theoretical and experimental results, Can. Bull. Fish. Aquat. Sci., 214, 521-559, 1986.

O'Brien, M. C., Macdonald, R. W., Melling, H., and Iseki, K.: Particle fluxes and geochemistry on the Canadian Beaufort Shelf: Implications for sediment transport and deposition, Cont. Shelf Res., 26, 41–81, doi:10.1016/j.csr.2005.09.007, 2006.

O'Brien, M. C., Melling, H., Pedersen, T. F., and Macdonald, R. W.: The role of eddies and energetic ocean phenomena in the transport of sediment from shelf to basin in the Arctic, J. Geophys. Res., 116, C08001, doi:10.1029/2010JC006890, 2011.

Pickart, R. S.: Shelfbreak circulation in the Alaskan Beaufort Sea: Mean structure and variability, J. Geophys. Res., 109, C04024, doi:10.1029/2003JC001912, 2004.

Reynolds, R. A., Stramski, D., Wright, V. M., and Woźniak, S. B.: Measurements and characterization of particle size distributions in coastal waters, J. Geophys. Res., 115, C08024, doi:10.1029/2009JC005930, 2010.

Reynolds, R. A., Stramski, D., and Neukermans, G.: Optical backscattering by particles in Arctic seawater and relationships to particle mass concentration, size distribution, and bulk composition, Limnol. Oceanogr., 61, 1869–1890, doi:10.1002/lno.10341, 2016.

Timmermans, M. L., Garrett, C., and Carmack, E.: The thermohaline structure and evolution of the deep waters in the Canada Basin, Arctic Ocean, Deep-Sea Res. I, 50, 1305–1321, 2003.

Sallon, A., Michel, C., and Gosselin, M.: Summertime primary production and carbon export in the southeastern Beaufort Sea during the low ice year of 2008, Polar Biol., 34, 1989–2005, doi:10.1007/s00300-011-1055-5, 2011.

Spall, M. A., Pickart, R. S., Brugler, E. T., Moore, G. W. K., Thomas, L, Arrigo, K. R.: Role of shelfbreak upwelling in the formation of a massive under-ice bloom in the Chukchi Sea, Deep Sea Res. II, 105, 17–29, doi:10.1016/j.dsr2.2014.03.017, 2014.

Stramska, M. and Stramski, D.: Variability of particulate organic carbon concentration in the north polar Atlantic based on ocean color observations with Sea-viewing Wide Field-of-view Sensor (SeaWiFS), J. Geophys. Res., 110, C10018, doi:10.1029/2004JC002762, 2005.

Stramski, D. and Kiefer, D. A.: Light scattering by microorganisms in the open ocean, Prog. Ocenogr., 28, 4, 343–383, doi.org/10.1016/0079-6611(91)90032-H, 1991.

Stramski, D., Reynolds, R. A., Babin, M., Kaczmarek, S., Lewis, M. R., Röttgers, R., Sciandra, A., Stramska, M., Twardowski, M. S., Franz, B. A., and Claustre, H.: Relationships between the surface concentration of particulate organic carbon and optical properties in the eastern South Pacific and eastern Atlantic Oceans, Biogeosciences, 5, 171–201, doi:10.5194/bg-5-171-2008, 2008.

Stroeve, J. C., Markus, T., Boisvert, L., Miller, J., and Barrett, A.: Changes in Arctic melt season and implications for sea ice loss, Geophys. Res. Lett., 41, 1216–1225, doi:10.1002/2013GL058951, 2014.

Tremblay, J.-É., Simpson, K., Martin, J., Miller, L., Gratton, Y., Barber, D., and Price, N. M.: Vertical stability and the annual dynamics of nutrients and chlorophyll fluorescence in the coastal, southeast Beaufort Sea, J. Geophys. Res., 113, C07S90, doi:10.1029/2007JC004547, 2008.

Tremblay, J.-É., Bélanger, S., Barber, D. G., Asplin, M., Martin, J., Darnis, G., Fortier, L., Gratton, Y., Link, H., Archambault, P., Sallon, A., Michel, C., Williams, W. J., Philippe, B., and Gosselin, M.: Climate forcing multiplies biological productivity in the coastal Arctic Ocean, Geophys. Res. Lett., 38, L18604, doi:10.1029/2011GL048825, 2011.

Williams, W. J. and Carmack, E. C.: Combined effect of wind-forcing and isobath divergence on upwelling at Cape Bathurst, Beaufort Sea, J. Mar. Res., 66 (5), 645–663, doi:10.1357/002224008787536808, 2008.

Williams, W. J., Carmack, E. C., Shimada, K., Melling, H., Aagaard, K., Macdonald, R. W., Ingram, R. G.: Joint effects of wind and ice motion in forcing upwelling in Mackenzie Trough, Beaufort Sea, Cont. Shelf Res., 26, 2352–2366, 2006.

Williams, W. J., Melling, H., Carmack, E. C., Ingram, R. G.: Kugmallit Valley as a conduit for cross-shelf exchange on the Mackenzie Shelf in the Beaufort Sea, J. Geophys. Res., 113, C02007, doi:10.1029/2006JC003591, 2008.

Woźniak, S. B., Stramski, D., Stramska, M., Reynolds, R. A., Wright, V. M., Miksic, E. Y., Cichocka, M., Cieplak, A. M.: Optical variability in relation to particle concentration, composition, and size distribution in the nearshore marine environment at Imperial Beach, California, J. Geophys. Res., 115, C08027, doi:10.1029/2009JC005554, 2010.

Yang, J.: Seasonal and interannual variability of downwelling in the Beaufort Sea, J. Geophys. Res., 114, C00A14, doi:10.1029/2008JC005084, 2009.

Biogeosciences Discuss., https://doi.org/10.5194/bg-2018-261
Manuscript under review for journal Biogeosciences
Discussion started: 21 June 2018

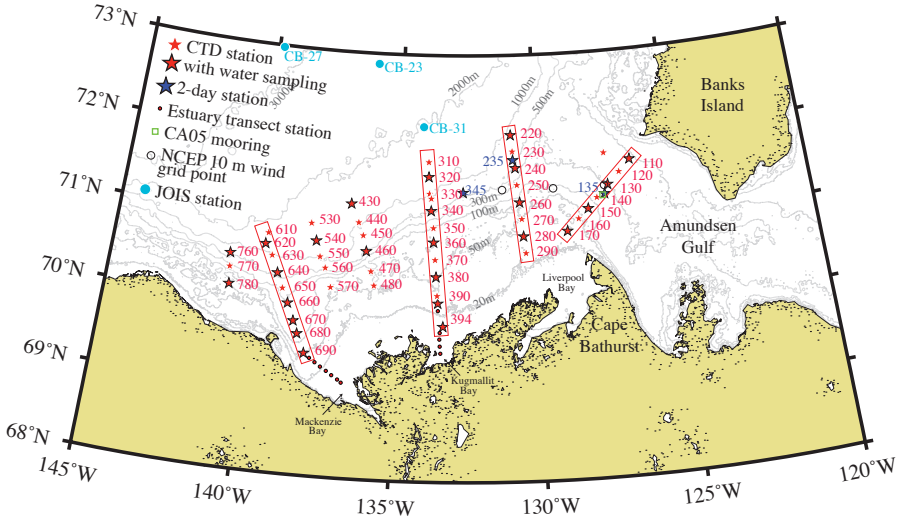

Figure 1. Map of study area with stations sampled along transect lines 100 to 700 during the Malina expedition in 2009. Rosette water sampling was conducted on the 28 stations marked by stars with black borders. Black circles are the three locations selected for NCEP 10 m winds. The green square near station 140 indicates the location of the long-term mooring CA05 with a current meter at 178 m or 202 m depth. The cyan circles mark the locations for three of the profiles shown in Fig. 12. The fourth station, CB-21, was located 1° north of CB-27.

Biogeosciences Discuss., https://doi.org/10.5194/bg-2018-261
Manuscript under review for journal Biogeosciences
Discussion started: 21 June 2018

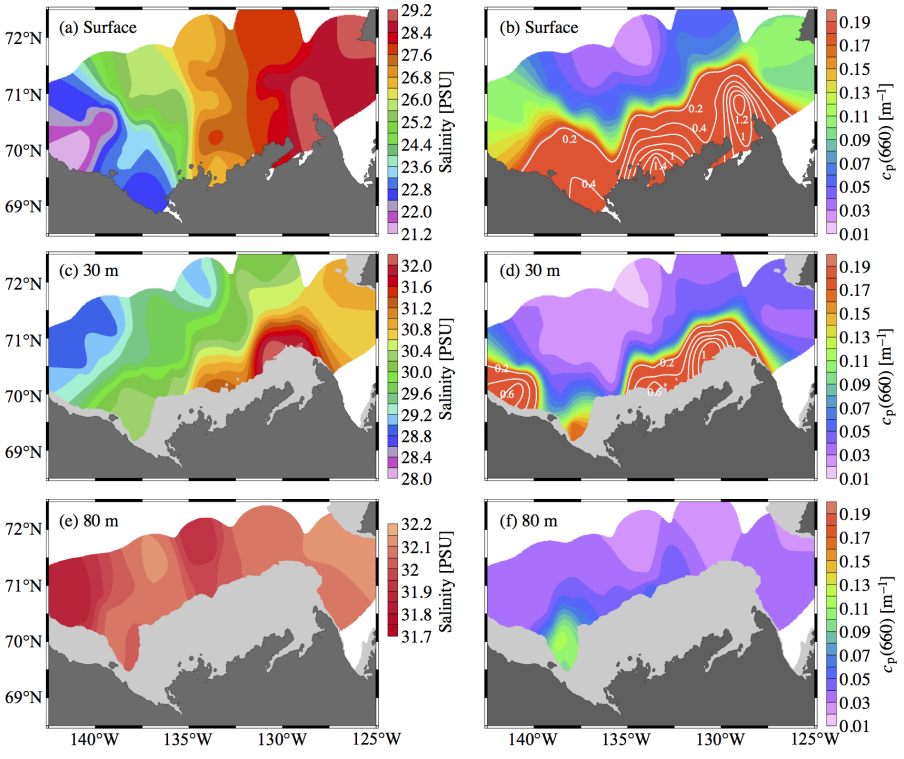

Figure 2. Surface fields of water salinity (left panels) and particulate beam attenuation coefficient at 660 nm, $c_p(660)$, (right panels) for (a–b) surface, (c–d) 30 m depth, and (e–f) 80 m during the MALINA 2009 expedition.

Biogeosciences Discuss., https://doi.org/10.5194/bg-2018-261
Manuscript under review for journal Biogeosciences
Discussion started: 21 June 2018

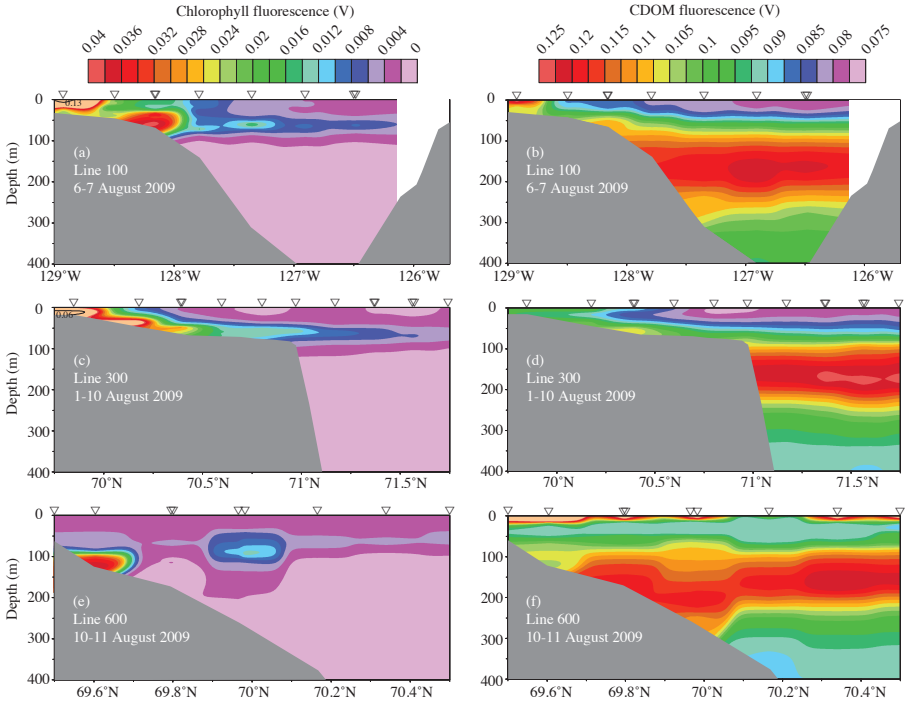

Figure 3. Voltage readings from the chlorophyll fluorometer (left panels) and CDOM fluorometer (right panels) for transects (a–b) 100, (c–d) 300 and (e–f) 600.

Biogeosciences Discuss., https://doi.org/10.5194/bg-2018-261
Manuscript under review for journal Biogeosciences
Discussion started: 21 June 2018

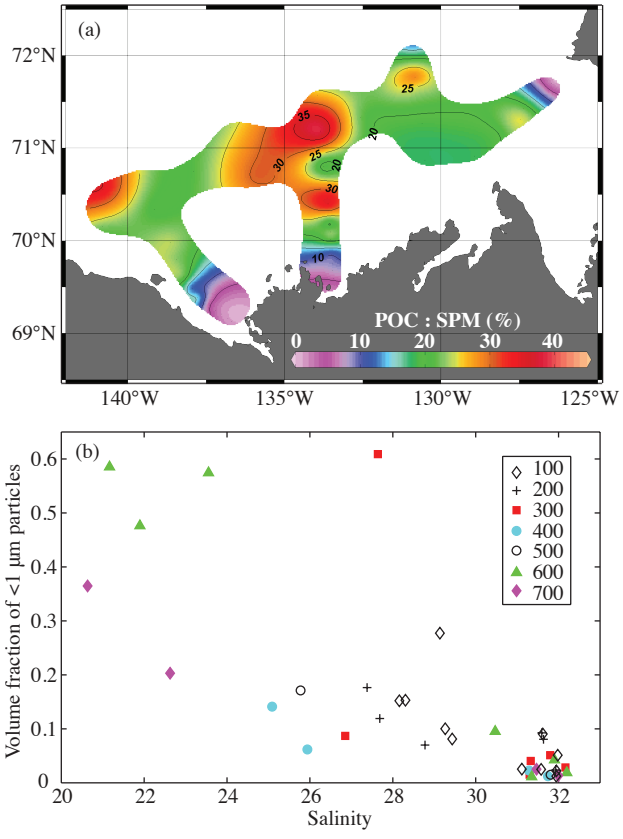

Figure 4. (a) POC to SPM ratio for surface samples within the study area and (b) relationship between volume fraction of particles less than 1 μm in diameter to total particle volume between 0.7 μm and 120 μm with salinity measured with a Beckman Coulter Multisizer 3 during the MALINA 2009 expedition.

Biogeosciences Discuss., https://doi.org/10.5194/bg-2018-261
Manuscript under review for journal Biogeosciences
Discussion started: 21 June 2018

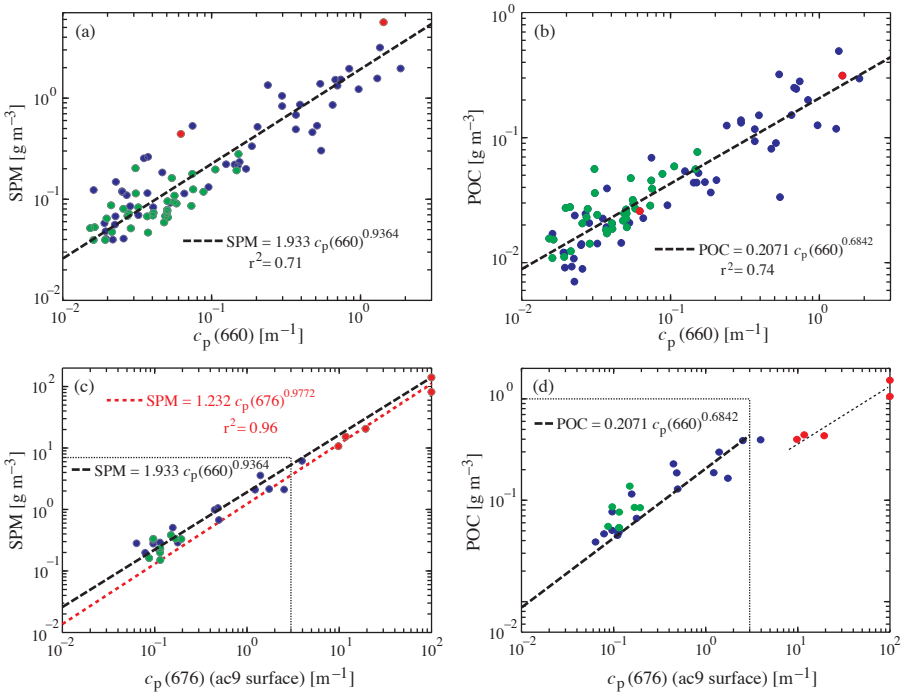

Figure 5. Relationship between SPM and POC to the particulate beam attenuation coefficient at 660 nm based on measurements from *CCGS Amundsen* during the MALINA expedition in 2009 (a–b) and with the particulate beam attenuation coefficient at 676 nm measured with the AC-9 from the barge (c–d) (the latter data contain only surface samples). The dotted squares in (c) and (d) indicate axes limits in (a) and (b), respectively. The colors of the data points indicate POC/SPM categories: mineral-dominated (red), mixed (blue), and organic-dominated (green).

Biogeosciences Discuss., https://doi.org/10.5194/bg-2018-261
Manuscript under review for journal Biogeosciences
Discussion started: 21 June 2018

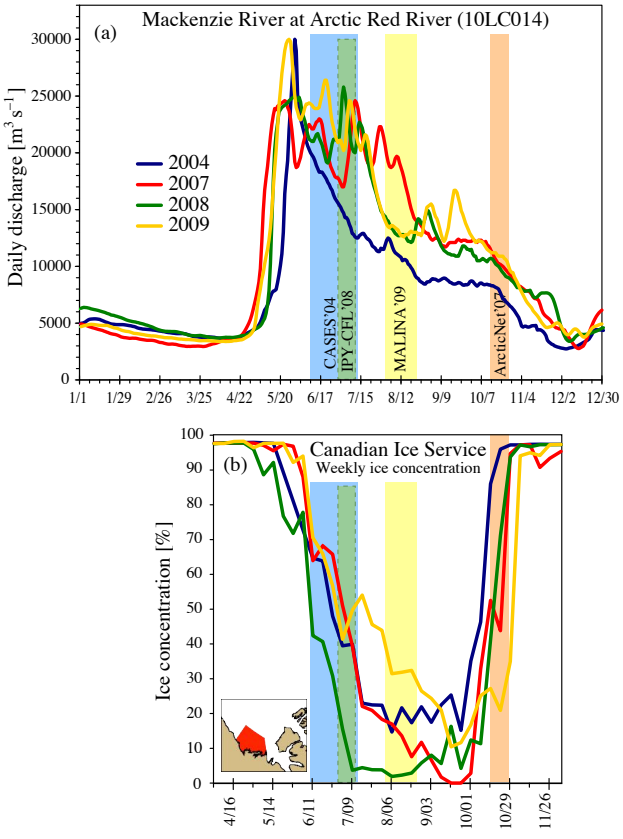

Figure 6. (a) Daily discharge for the Mackenzie River at the Arctic Red River location (10LC014). Data obtained from Environment Canada. (b) Weekly ice coverage for the Mackenzie Shelf area calculated using IceGraph 2.0 provided online by the Canadian Ice Service. Time periods for the four expeditions considered in this study are also indicated in color shades.

Biogeosciences Discuss., https://doi.org/10.5194/bg-2018-261
Manuscript under review for journal Biogeosciences
Discussion started: 21 June 2018

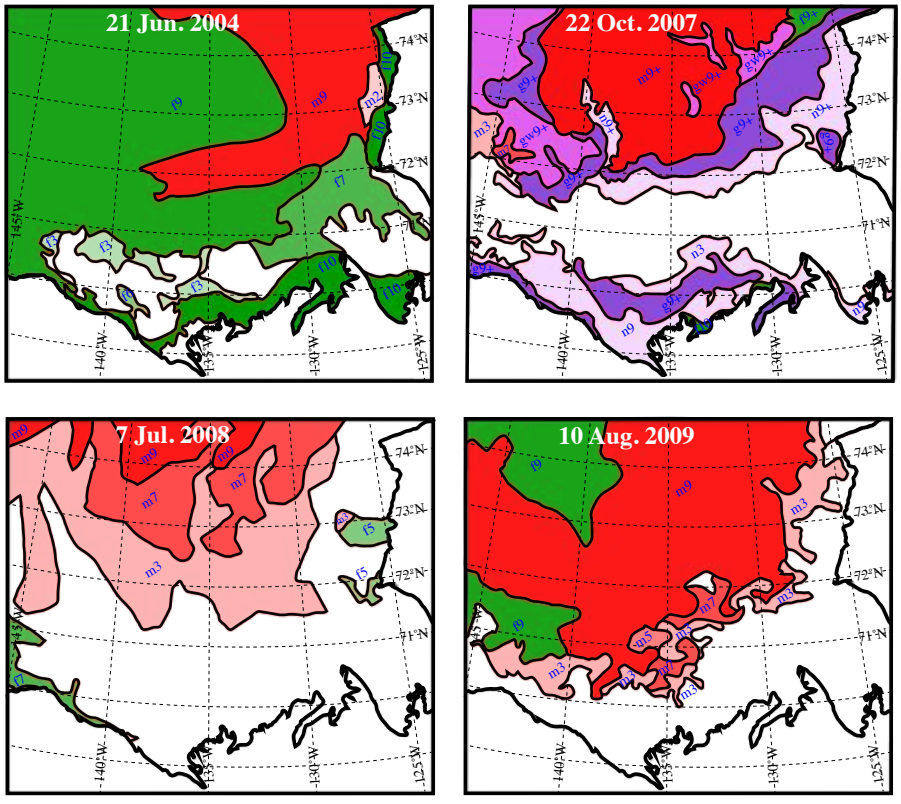

Figure 7. Ice coverage data from the Canadian Ice Service. The blue labels denote areas of first-year ice ('f'), multi-year ice ('m') and new ice types: nilas ('n'), grey ice ('g'), grey-white ice ('gw'), while numbers that follow indicate ice concentration in tenths (9+ indicates > 90 %). The areas of the three ice types are also associated with colors; green for first-year ice, red for multi-year ice and purple for the new ice types, while the color shade relates to concentration.

Biogeosciences Discuss., https://doi.org/10.5194/bg-2018-261
Manuscript under review for journal Biogeosciences
Discussion started: 21 June 2018

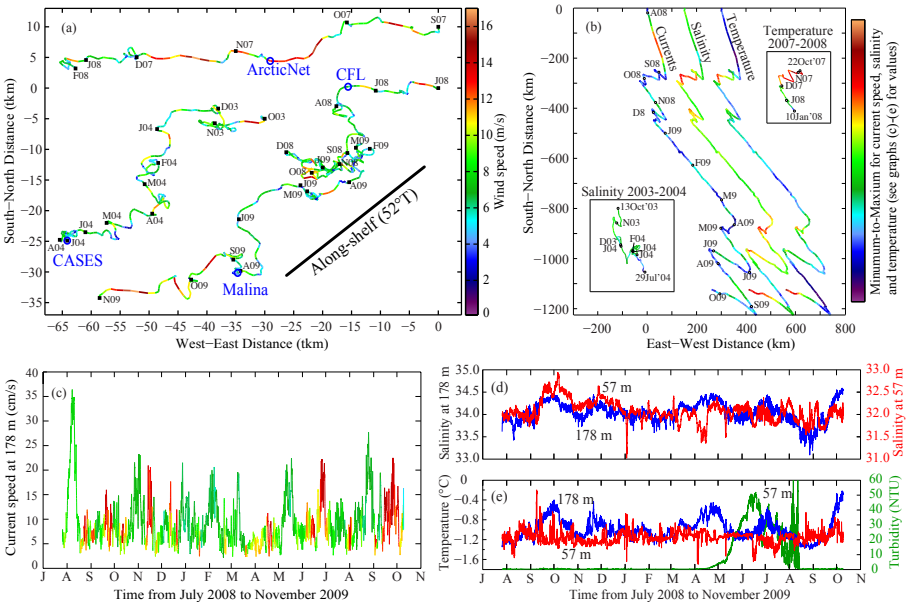

Figure 8. Progressive vector plots of (a) daily average wind (NCEP, 10 m) and (b) currents from mooring CA05, with insets for 2003–2004 and 2007–2008 data. Colors in (a) indicate daily average wind speeds shown in color bar, while in (b) the colors of each plot indicate either current speed, salinity or temperature as denoted next to the lines and shown in more detail in (c)–(e). The start of each month is indicated. For the insets in (b), showing 2003–2004 and 2007–2008 data, the colors indicate either temperature or salinity as denoted. The four blue circles in (a), marking 1 July 2004, 20 October 2007, 8 July 2008, and 7 August 2009, respectively, show the approximate times of the ship-based transect sampling across the Mackenzie shelf break used in this study. The black line shows the direction along the shelfbreak referenced to True North. Time series for 2008–2009 for (c) current speed (colors are current directions), (d) salinity at two depths on the mooring (note different scale), and (e) temperature at two depths and turbidity (green line) at 57 m (the turbidity at 178 m remained near zero throughout the time series).

Biogeosciences Discuss., https://doi.org/10.5194/bg-2018-261
Manuscript under review for journal Biogeosciences
Discussion started: 21 June 2018

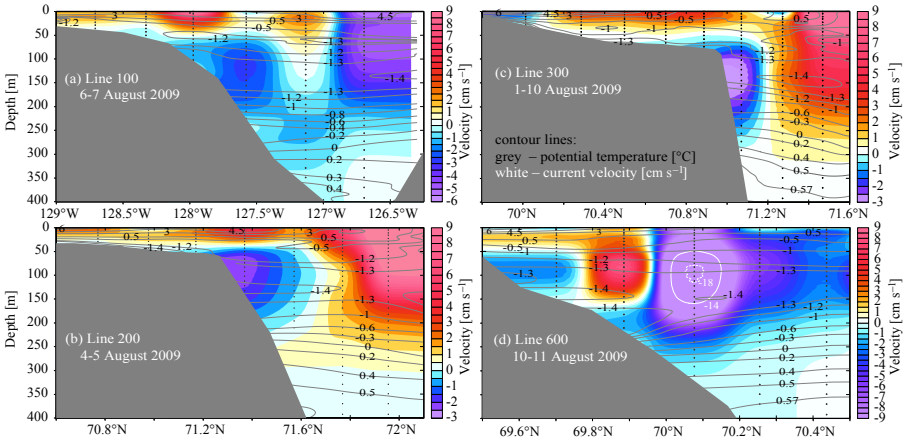

Figure 9. Sections of geostrophic current velocity (colors and white contours) perpendicular to transect lines 100 (a), 200 (b), 300 (c), and 600 (d). Note the changes in scale. The grey contour lines are for potential temperature. Geopotential heights were referenced to 500 m. Positive current values are generally for the direction perpendicular to the transect lines (see Figure 1) either towards northwest (a) or west (b–c) or southwest (d).

Biogeosciences Discuss., https://doi.org/10.5194/bg-2018-261
Manuscript under review for journal Biogeosciences
Discussion started: 21 June 2018

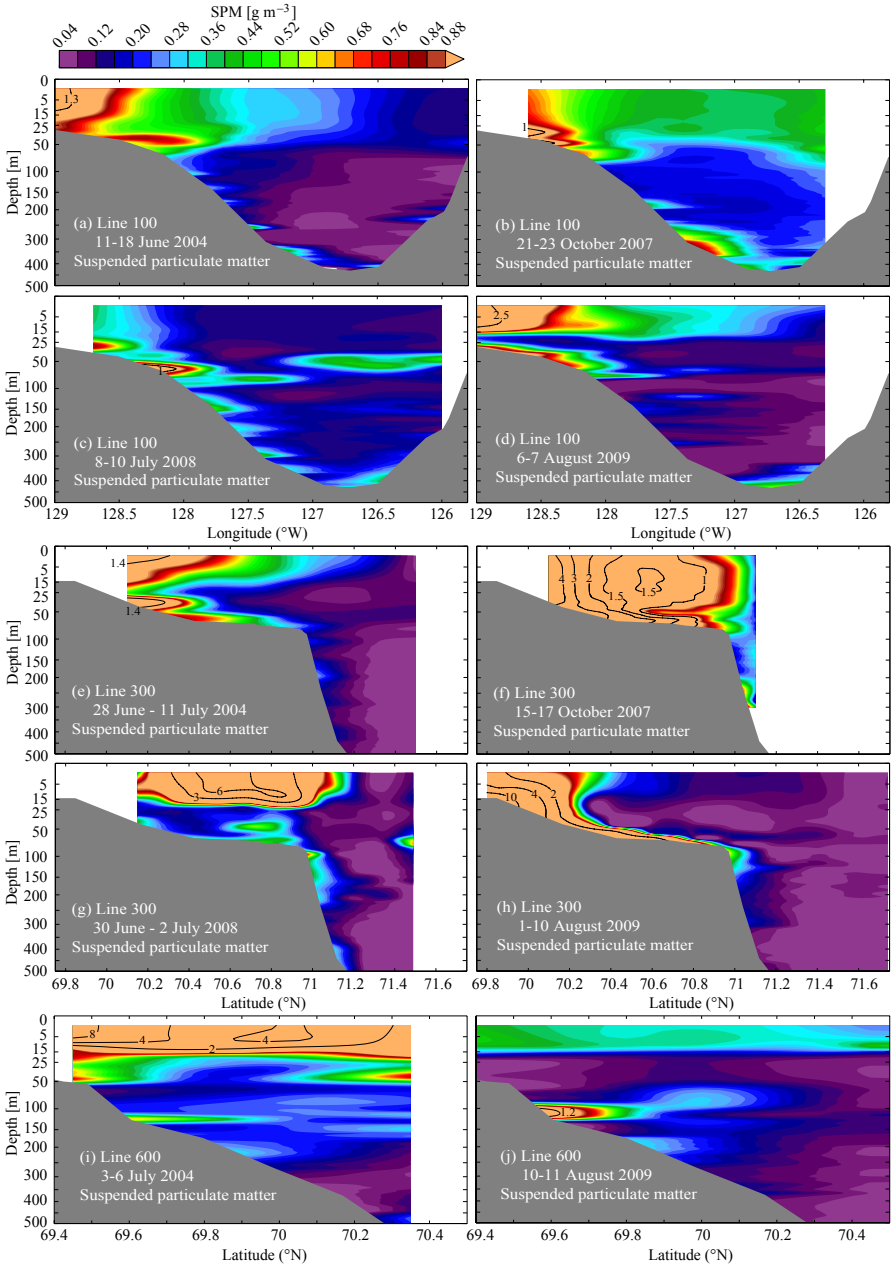

Figure 10. Concentration of suspended particulate matter, SPM, calculated from measurements of particulate beam attenuation coefficient at 660 nm, $c_{\mathrm{p}}(660)$, using Eq. 2 for lines 100, 300 and 600 during different field campaigns in 2004, 2007, 2008, and 2009, as indicated.

Biogeosciences Discuss., https://doi.org/10.5194/bg-2018-261
Manuscript under review for journal Biogeosciences
Discussion started: 21 June 2018

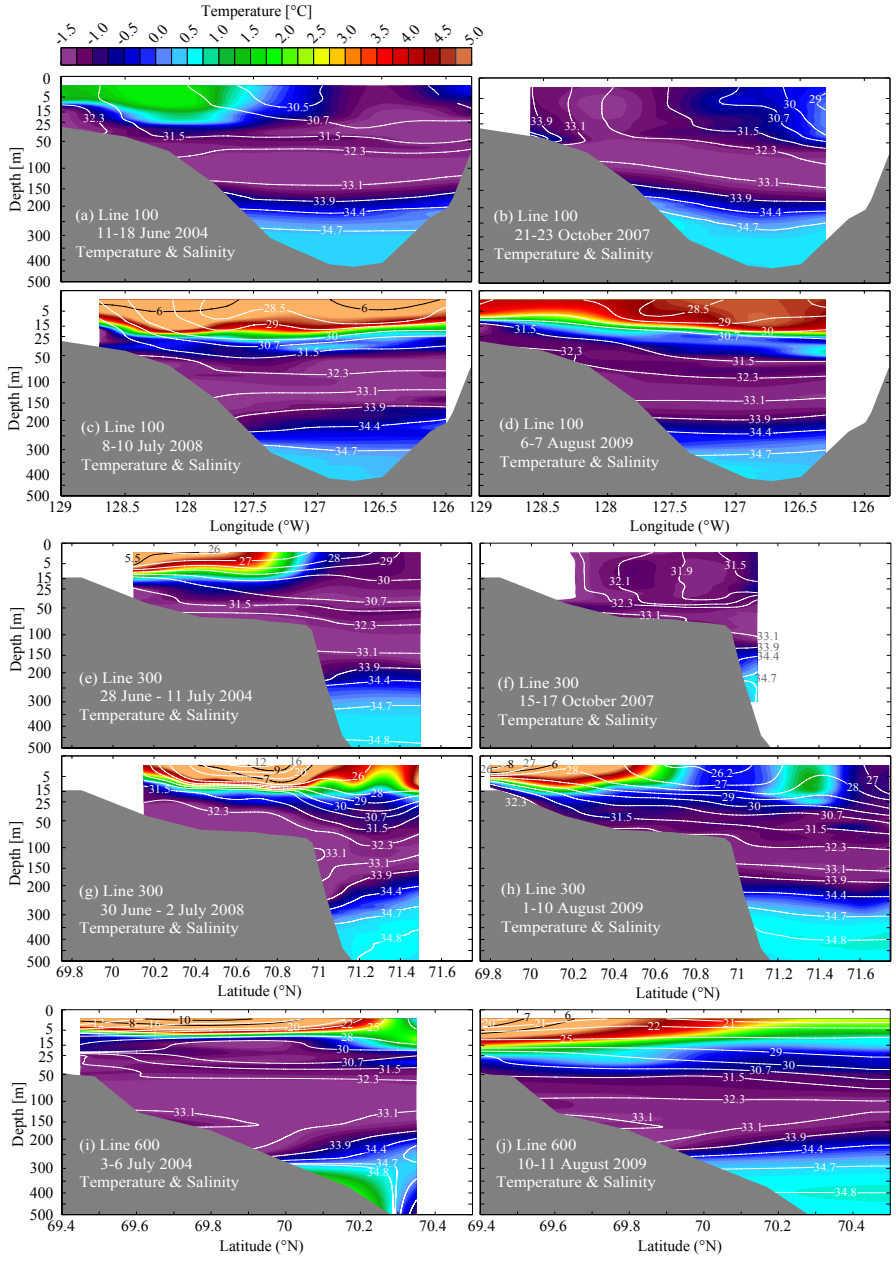

Figure 11. As Fig. 10 but for water temperature (colors) and salinity (contour lines).

Biogeosciences Discuss., https://doi.org/10.5194/bg-2018-261
Manuscript under review for journal Biogeosciences
Discussion started: 21 June 2018

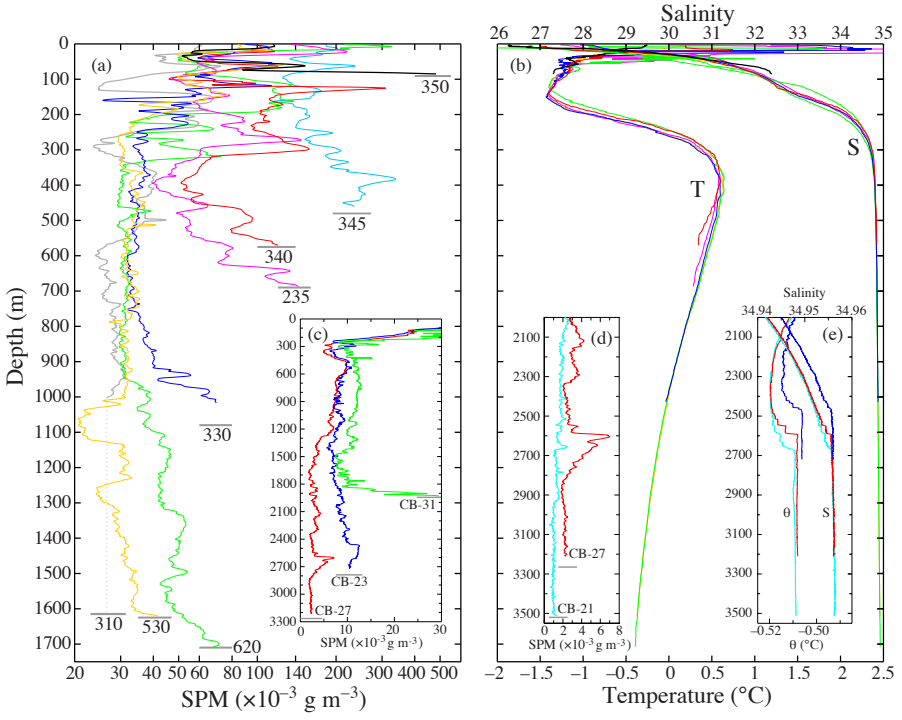

Figure 12. Vertical profiles of (a) suspended particulate matter, SPM, calculated from particulate beam attenuation coefficient at 660 nm, $c_p(660)$, and (b) temperature, T, and salinity, S, at selected "deep" stations. Inserts (c) and (d) show transmissometer data (converted to SPM using Eqs. 1–2) that were collected in Canada Basin during 21–23 September 2009 and made available by the Beaufort Gyre Exploration Program based at the Woods Hole Oceanographic Institution (http://www.whoi.edu/beaufortgyre) in collaboration with researchers from Fisheries and Oceans Canada at the Institute of Ocean Sciences. Insert (e) shows a close up of the potential temperature, θ, and S for CB-23, CB-27 and CB-21 at the interface to the Canada Basin Bottom Water layer. Grey horizontal lines indicate bottom depths and are underlain by station numbers (see Fig. 1 for locations).